Transient Relaxation Mechanisms in Elongated Melts and Rubbers Investigated by Small Angle Neutron Scattering

François Boué
Laboratoire "Léon Brillouin" Centre d'Energie Nucléaire de Saclay,
91191 Gif-sur-Yvette Cedex/France

The dynamics of polymer melt can be investigated by observing the return to isotropic state of a piece of melt after a sudden deformation, maintained during all the process of relaxation (a step-strain). This method of transient relaxation is applied to small angle neutron scattering measurements. The very large domain of time which is covered using the time temperature superposition allows to test the different models of dynamics, mainly the Rouse model (chains are assumed to behave as if they were free) and the tube-reptation model, successfully applied for the description of entangled polymer. The possible form factors for oriented polymers are also discussed for the melt as well as for rubbers. The labelling technique (deuteration) is very flexible and allows to observe chains of given molecular weight inside matrices of chains of another molecular weight.

Advances in Polymer Science 82

1 Introduction

The material studied here is a particular solid: a polymer melt, i.e. a polymer in the bulk state above the glass transition temperature T_g and crystallisation temperature T_s. Because the chains are long and entangled, the maximum characteristic time is also very long. It is easy to reach considerably lower values, as in the experiment described here, in the lower time range: thus the material behaves macroscopically as a solid. In the upper time range, one approaches the maximum relaxation time and the material begins to behave macroscopically as a liquid. A few results will also be given on cross-linked melts (i.e. rubbers) which will never behave macroscopically as a liquid because of the permanent crosslinks. Conveniently for Small Angle Neutron Scattering (SANS) measurement the sample (polystyrene, PS) is quenched in the glassy state; PS does not crystallize, it just freezes in the melt state without any conformational change. Flows of solutions can be used in SANS for determining the dynamics of solutions (see end of section 2.1); however, data on this methods will not be discussed here. We basically consider the dynamics of a chain in a polymer melt.

Briefly, the experiment is the following: the sample is prepared in an isotropic state and contains labeled (deuterated) chains. It is then deformed as fast as possible and maintained under constant conditions (length, temperature). The small angle neutron scattering — due to the presence of the deuterated chains — is recorded for each value of the time t elapsed since the end of the stretching. This gives the form factor of the single chain as a function of t, denoted as $S_t(q)$. If the duration of the stretching is short compared to the time t, the deformation history is equivalent to a step strain. A typical variation of the stress with t is given in Fig. 1; the different regimes will be described later; the longest relaxation time is denoted as T_{ter} and was measured in some of the experiments. As the time t increases, the material returns to the isotropic state. Thus, $S_t(q)$ returns to the isotropic form factor for $t \gg T_{ter}$, i.e. the dynamics are observed via the return to equilibrium of a deformed system under the effects of the thermal fluctuations. This use of static SANS for dynamics appears as a *very powerful* tool, for several reasons:

(i) it is well suited to the melt as it can use nuclear labeling (deuteration) which does not cause demixtion, because the Flory factor χ between deuterated and hydrogenated

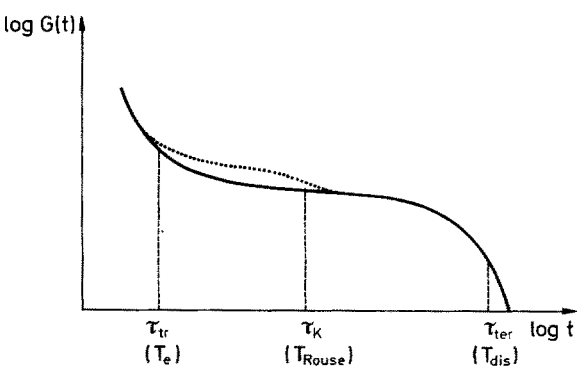

Fig. 1. Schematic variation of the modulus G(t) with time after a step deformation, for a small elongation ratio (solid line) and large one (dotted line)

species is very weak. The labeling allows also to observe chains of a given molecular weight diluted among chains with different molecular weights.
(ii) measurements can be precise or reasonably fast for a melt such as polystyrene because a large fraction of deuterated species can be used, which gives a large scattering signal [1], when χ can be neglected (see Ref. 62).
(iii) it covers a large part of the submolecular range of the scattering vector q for chains with molecular weights M which are relatively easily synthesized and handled and cover completely the range of scientific and industrial interest. Namely, q range from $5 \cdot 10^{-3}$ Å^{-1} to $5 \cdot 10^{-1}$ Å^{-1} and M from some thousands to $2 \cdot 10^6$.
(iv) it allows to study times t which are too long to be covered by the inelastic techniques observing the fluctuations of the system at equilibrium.

Other techniques used for dynamics do not combine these advantages. For example, light scattering fulfills only (iii) within a different range of q but not (i); X-ray scattering obeys (ii), (iii), and (iv) but again not (i). For optical techniques, (i) is fulfilled such that they can be applied to melts (see Sect. 15), but the advantage (iii) disappears. Inelastic neutron scattering combines (i), (i), and (iii) but excludes (iv).

The SANS method for dynamics has been developed while other techniques have also been much improved. This led to a renewal of the interest on the subject, also because at the same time new and stimulating theories were developed. The masterpiece of this theoretical work is the tube [2]-reptation [3] model: the main idea of reptation is to assume that, in the point of view of the dynamics of each chain, the obstacles formed by the other chains create a tube inside which the chain is constrained: it has then to *disengage* the tube by its two ends via a one-dimensionnal motion along the centre line of the tube; this gives a maximum relaxation time T_{dts} proportional to M^3 (de Gennes, 1971), and well separated from the shorter times of the relaxation spectrum. This 3rd power law is a great advantage of the theory, as the old Rouse model only predicts M^2. Specifications on the tube itself are not directly derived by the genuine theory; but as far as the effect of its fluctuations tends to a permanent constraint at long times, for large enough T_{dis}, i.e. long enough chains, the relevant process will be disengagement. This theory allows for a large crossover range of time and molecular weight, before reaching the pure disengagement regime. This idea has been precisely exploited in the Doi-Edwards model for melts [4]. The crossover is described by imposing a constant size D of the tube diameter, without knowing how this could arise: thus the model of dynamics is not selfconsistent. However, the fit of mainly rheological data is then possible and furnishes a value for D for each polymer. It is expected, as often in physics, that the crossover ranges are different depending on the physical quantity measured. The crossover in time is escaped in some experiments which measure the self diffusion coefficient; the time scales are then much larger than the maximum time of the chain. The mass crossover must still exist for the selfdiffusion but seems to lie at small values; the disengagement prediction $D \propto M^{-2}$ is verified in the range of accessible high masses. The situation is different for other physical quantities: for example, the maximum time for viscoelastic quantities is proportional to $M^{3.4}$, instead of M^3. This can be explained by a crossover effect [5] such that the test of the M^3 dependence would require extremely high masses ($> 10^7$ for polystyrene), which are difficult to synthesize as well as to handle. Quantitative specifications for the tube then become important, at least in commercial applications for which the molecular weight is not so large. These latter also involve

very polydisperse samples for which the crossover regime can be very complicated. One interesting feature of the experiments reviewed here is the exploration of this eventual crossover regime in time, which can give new information on the still unknown motions involved at that stage. It will be seen that the limit model behaviour of an ideal free chain for the shortest time can be in agreement with measured data, while in the upper range the limit of pure disengagement is less obviously checked so far, and should at least lead to modifications of the simple specifications on the tube contained in the model of Doi-Edwards.

All cases, let us insist, will benefit from the huge advantage of observing the motions at different scales of length, or in other words, together the t dependence, via the q dependence.

Three parts will appear in the review. First the background of the experiment: technical remarks and the possible extensions or alternatives for using SANS in dynamics (Sect. 2), the background of the present interpretation of the data (Sect. 3), and a brief recall of the Doi-Edwards model. Second, a detailed description is given of the different characterizations of the (q, t) dependence, radius of gyration, asymptotic laws and comparison of the form factor with some calculated expressions; some recent results on crosslinked melts and mixtures of different molecular weights will be presented. The third part contains additional remarks on other more detailed approaches.

2 Technical and Theoretical Background

2.1 The Use of Elastic SANS for Polymer Dynamics

The different ways of investigating the polymer dynamics by elastic neutron scattering is focussed upon in this section, especially the case of the "step strain + quenching" method, as it is currently the only method used for uncrosslinked melts. A few other methods, mentioned in the text, are presently being developed (also see review by Oberthur [6]).

The Deformation History. Polymer dynamics can be investigated by SANS via special phenomena such as demixtion [7] observed by X-rays [8] or crystallization. A more direct way is simply to observe a sample mechanically displaced out of equilibrium. A classical approach used in other techniques is a *steady* deformation, characterised by a constant rate of deformation $s = 1/L\ dL/dt$, where L is a distance. The investigation in time is related to the dependence on s. Other procedures involve time-dependent deformation histories, which relate to the actual time: typical cases are a periodic deformation, e.g. oscillatory, and a stepstrain deformation. A time analysis is then needed. In the case of a periodic deformation, one can divide the period $2\pi/\nu$ into small intervals of phase ψ, $\psi + \Delta\psi$, within which $S_{\psi,\nu}(q)$ is measured. In the case of stepstrain there is only one time parameter, the time t elapsed after the stepstrain which will be divided into short intervals to measure $S_t(q)$.

The deformation can be stretching or shear. In the case of very liquid melts or solutions, a flow cell can be used (Couette flow or elongational cell), which is specially convenient for steady deformation.

Glass Transition: Time Magnification and Quenching. Polymers are glass-forming materials. If no crystallization occurs, this means that the spectrum of relaxation time depends on temperature via the difference $T - T_g$, where T_g is the glass transition temperature. For all kinds of glasses the dependence is similar: all the times of the spectrum are multiplied by the same factor $a_T = f(T - T_g)$ [12]. The closer to T_g, the larger is the variation of f; a_T can range over several decades (six is easily achieved for polymers). As glass transition freezes the dynamics, it allows a quenching of the relaxation process, which makes it convenient to observe the sample a long time, as it could be necessary with SANS.

Different Possible Time Analysis. At a given temperature the whole spectrum spreads for long chains also over several decades. Finally, a combination must be made between: the relevant physical time of the spectrum, the temperature, the use of quenching, and the counting time needed. There are three ways to obtain $S_i(q)$ after stepstrain deformation:

a) Direct acquisition in situ. One acquires the data for an interval $(t, t + \Delta t)$, where Δt is the counting time needed for a full run but is small compared to t. Thus, the minimum t is proportional to the minimum counting time Δt_{min} needed for a reasonably large intensity recorded at each q.

b) Repeated acquisition in situ. Δt is taken shorter than Δt_{min} and the deformation is repeated several times (allowing for relaxation of the sample between two successive times). The minimum t is related to the minimum time of acquisition of the electronics of the multidetector and time channel system.

c) Quenching. One eliminates the limit of the counting time and does not need to relax the sample in situ. One sample may be used for each value of t, or the same reheated several times (both methods have been used). The duration of quenching and of eventual reheating must be short compared to t.

Exactly the same three methods may be used for any time-dependent deformation (e.g. also the oscillatory one). Quenching is easier for T not far from T_g. It can also be used to quench a steady deformation of a melt. However, it is not suitable for solutions nor crystallizing polymers. Direct acquisition in situ requires to observe a long time period within the spectrum of a long chain, or to work very close to T_g to magnify all times of the spectrum; this requires a precise temperature control, as a_g depends strongly on $T - T_g$. Repeated acquisition is suitable for times much shorter than the maximum time; this is especially convenient for rubbers for which this latter is infinite.

The Anisotropy of Scattering. In all experiments reported here the sample is oriented in order to have a scattering depending on the angle φ between the scattering vector q and the principle axis of the deformation (here generally the stretching axis). This supplies much information for all directions φ, but involves long counting times (see Sect. 12). It is possible to align the drawing axis of the sample with the beam axis, which gives an isotropic scattering, for example with an equibiaxial extension, or a uniaxial one if the sample is cut perpendicularly to the stretching axis $\vec{S}$ into narrow bands and consecutively piled vertically with their cross section perpendicular to the beam.

Temperature control. This is generally achieved via a fluid. For acquisition in situ, the temperature equipment must be transparent to neutrons; a gas (air) is then suitable for thermalising. If the acquisition is done after quenching, any system can be used; the use of a liquid (liquid salt or non-swelling oil (silicone)) has the advantage, compar-

ed to air, to allow fast reheating and to prevent the sample to flow under gravity during long time periods by matching the density of the liquid to the one of the melt. A complication arises when accuracy of the control is needed on a large length scale, as for uniaxial stretching which makes the samples very long. A detailed discussion of such experiments is given in Refs. [9] and [10].

Making an Unstrained Sample. If one uses a "solid" sample, i.e. neither a very liquid melt nor a solution, one has to ensure a perfectly unstrained state before the deformation. For melts this is related to the moulding, which should not induce too large strains and, mainly, to the annealing. An artefact from uncorrect annealing will appear at relaxation times of the order of the annealing time, such that studies at longer times need more careful annealing. The duration of the annealing will increase with the terminal, relaxation time i.e. considerably for molecular weights over 10^6 (typically one day at 180 °C). Under these conditions a new difficulty arises from the chemical degradation. First, the degradation time becomes of the order of the annealing time; second, large chains are much more sensitive to degradation than the smaller chains. This has so far limited our exploration of long times; progress has been made recently.

Currently Performed Experiments. Flow experiments with equipment similar to the Schlumberger elongational viscometer have been attempted, but encountered many difficulties; an elongational "cross cell" system (same flow as the Taylor four-roll-mill) is being developed [11]. Shear flow has been studied more extensively in a Couette viscometer (see Ref. [6] for review). A periodic oscillatory uniaxial deformation has been recently started on PDMS rubbers [6]. Up to now the range of available time

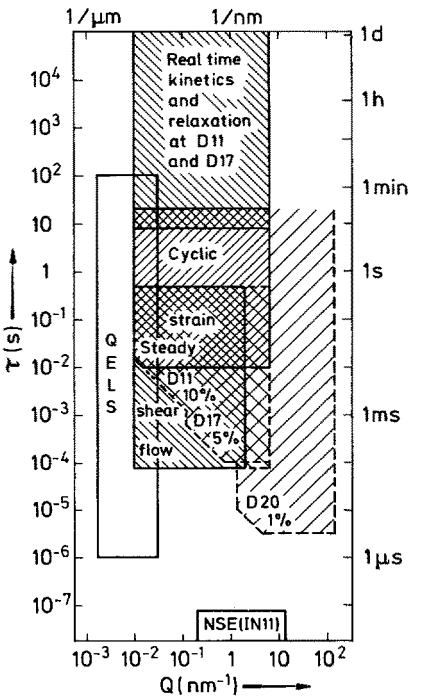

Fig. 2. Time (τ) and scattering vector (Q) range for various scattering experiments on dynamics: SANS ILL spectrometers D11 and D17: relaxation after stepstrain, cyclic experiments, steady couette shear. Elastic neutron scattering ILL spectrometer D20, also real time experiment. Neutron Spin Echo (NSE) ILL spectrometer, inelastic measurement and classical quasielastic light scattering (QELS) (from Ref. [6])

($>10^{-2}$ sec) is large compared with the molecular times expected for this materials (10^{-10}–10^{-5} s). The orders of magnitude of time and scattering vectors are given in Fig. 2 for these different experiments. The rest of the review is mainly devoted to stepstrain experiments involving quenching of uncross-linked, but also crosslinked, polystyrene. The whole set is reviewed in Sect. 4.

2.2 Theoretical Background of Melt Dynamics

For melts and concentrated solutions the current theory outlines the following: at short times, the Rouse model, in which the other chains only play the role of a viscous medium for individual chains, is accepted to fit all the data for polymer dynamics. Sufficiently long chains involve times longer than a threshold T* for which that model is clearly wrong: the chains are then called "entangled". The current idea is that the other chains now slow down the lateral motions of a particular chain above a typical distance much more strongly than its longitudinal motion which is still of the Rouse type. Then, for large enough chains only this latter motion is relevant; it is a "reptation" inside the obstacles due to the other chains imagined as a tube surrounding it. There is no theoretical explanation of this slowing down, i.e. of the typical size of the tube, as the collective dynamics are still unknown. Thus, the tube is not selfconsistent. The Rouse model uses Einstein's description of Brownian motion for each monomer and the entropic elasticity of the Gaussian chain (it fails, e.g., for distances smaller than the size, ϱ, of a set of a few monomer; this set is called the Rouse subchain). Reptation uses the same description. But, in addition, it needs an arbitrary description of the tube. Its typical diameter D can only be obtained from data on entangled material, in contrast to the friction coefficient ζ and the size ϱ which can be approached in monomeric or static experiments. There is an exception in semidilute solutions for which de Gennes proposed $D = \xi$ (correlation length), which exerts a certain concentration dependence (although some recent papers propose the existence of a second characteristic length in that range of concentration, see Adam and Delsanti). In concentrated solutions $\xi \propto c^2$, which gives the right dependence for the modulus.

For melts and concentrated solutions, Doi and Edwards presented a comprehensive model connecting the 3d Rouse model for the small scale with the tube model for the large scale ($r > D$). D can be taken as the radius of gyration of a Brownian subchain of molecular weight $M_e \propto D^2$. The Rouse model will then fail for $t > T^* = T_e = T_{Rouse}(M_e) \propto M_e^2$. Later on, the motion is uniquely a one-dimensional Rouse motion along the centre line of the tube; as predicted by de Gennes, a second and third process will appear. The second is an equilibration-fluctuation of the linear density along the central line of the tube, with the Rouse spectrum $\tau_p \propto (1/p^2)\,(M/M_e)^2$. In the third process the chain moves as a whole together with its centre of gravity along the tube centre line in a back-and-forth motion; each time one end approaches from the centre to the extremity of the tube it creates a new end part; the relaxation spectrum is then $\tau_p \propto (1/p^2)\,(M/M_e)^3$, p being an odd number only.

Doi and Edwards extended the model to the case of relaxation after deformation (in particular stepstrain). As already remarked by Daoudi, the length along the centre line at $t = T_e$ is then larger than the equilibrium length in the corresponding tube under isotropic conditions. Thus, the chain will retract inside the tube, which will

shorten. Before and after this process Doi and Edwards describe the medium as a rubber with a number of crosslinks proportional to the length of the part of the tube which has not yet relaxed. This allows to calculate the stress following the classical theories of rubber elasticity. The shortening of the tube and the retraction of the chain then allow to explain the decrease in stress for high deformation observed at a certain $\tau_k \propto M^2$, with exactly the right variation of λ. The stress can also be calculated for the last process (disengagement). Only the centre part of the tube remains deformed; its length is:

$$L(t) = L_0\mu(t)$$

with

$$\mu(t) = \Sigma_{p\,odd}(1/p^2)\exp(-p^2t/T_{dis})\,.$$

The number of active meshes is proportionnal to $\mu(t)$, which gives for the stress:

$$\sigma(t) = (\lambda^2 - 1/\lambda)\,G_N^0\mu(t)\,.$$

One can then take the mesh size equal to M_e; this gives, via the rubber model, the plateau modulus:

$$G_N^0 = kT/M_e\,.$$

M_e from the plateau modulus agrees with M_e from the time threshold for failure of the Rouse model ($T_e \propto M_e^2$) [12], such that the reptation model is consistent.

It still fails for the dependence upon molecular weight, $M^{3.4}$, (experimental) instead of M^3 (theoretical). Doi suggested that the main disengagement process is combined with the linear density fluctuation, as the two characteristic times proportional to $(M/M_e)^2$ and $(M/M_e)^3$ are close if M/M_e is not too large. The 3.4 in $M^{3.4}$ is an apparent exponent and should disappear for very long chains (for which data are not yet available).

However, it is not obvious that, even apart from that effect, the crossover is as sharp between the Rouse and pure reptation, as suggested in the Introduction. One way of expressing this relationship is to modify the tube theory by varying the tube diameter: this is called tube renewal. There are several possibilities: a first proposal was the effect of disengaging of other chains [13]; the effect is important for a long chain M embedded in shorter chains P (the characteristic time being M^2P^3) but not for all chains of same length (M^5!). In case of deformed systems it was noted that in the contraction process the other chains also contract, increasing the tube diameter, which in return lowers the retraction effect. Selfconsistent calculations have been proposed [14]. Also the fluctuations of linear density of the chain allows a first disengagement (this being the main relaxation effect for star polymers [15]). The effect of the molecular weight of the matrix on the relaxation of a chain of given weight (Refs. [16] and [17]; also see Sect. 11) can be explained by these modifications of the genuine theory. Other theories proposing leaks in the tube [18] or selfconsistent power laws [19] are currently being considered.

Still other possibilities exist; e.g., a concept revealing a weakness of the Doi-Edwards model: the modelization of the melt by a temporary rubber leads to the use of the classical rubber theory: this is known to encounter considerable discrepancies for actual rubbers (crosslinked melts). A slightly different description of a rubber would lead to greater motion of the crosslinks, and consequently of more extensive rearrangement of the tube constraints in the melt (see Sect. 13).

3 Loss of Affineness and Time Dependence

Here we describe the qualitative variation of the form factor with the scattering vector q (of modulus $|q| = q$) and the duration of relaxation t. The covered time range must also be defined, which is usually achieved by referring to the viscoelastic behaviour. Furthermore, different possibilities of data interpretation are suggested.

3.1 Loss of Affineness

In Fig. 3 $q^2S(q)$ is plotted against q. The dot-dashed line represents the isotropic form factor of a Gaussian chain, the dotted lines represent the totally affine representation explained later. For any value of t, the curves have the same following characteristics: in the parallel direction they start from a very small value of $q^2S(q)$ and increase when q increases; for large q they are close to the isotropic form factor. In the perpendicular direction they start at small q from a small value, increase to a maximum, and then decrease back towards the isotropic form factor. Actually the two directions reflect the same basic feature: as q increases (i.e. as the length scale decreases), the form factor appears closer to the one of the isotropic chain. In the parallel direction the function is always increasing, but in perpendicular direction there is a maximum; this maximum is not present in a S(q) vs q plot, but comes from an artefact of the $q^2S(q)$ representation in the range $1/q \sim R_g$. R_g is the radius of gyration, i.e. the global size of the chain. For $q \ll 1/R_g$, the form factor is nearly a constant, as would be the Fourier transform of a delta function, because the chain appears as a small point; S(q) can be understood as the number n(q) of scattering points in a sphere of radius 1/q. Thus, that number is equal to N and constant as long as 1/q is larger than the size of the chain, i.e. here $1/q \gg R_g$. Thus, $q^2S(q)$ increases in all directions for $qR_g < 1$; this regime corresponds to the increase of the perpendicular while this is not the case for the parallel direction in the available q range because $R_{g//}$ is too large: we have always $qR_{g//} \gtrsim 1$. The regime $qR_g > 1$ concerns the inside of the macromolecule. The number n(q) of scattering points thus starts to decrease. For an isotropic Gaussian chain, it decreases as $(1/q^2)$ (as $r \propto \sqrt{n}$), and $q^2S(q)$ is constant. For a deformed chain, n(q) is higher in the perpendicular direction, because the chain has been compressed, and smaller in parallel. When q increases, the curves return back to the isotropic curve; in parallel it produces an increase, in the perpendicular a decrease and consecutively a maximum appears the whole curve for the perpendicular direction. This return to isotropy at large q reflects the origin of the possibility of large recoverable

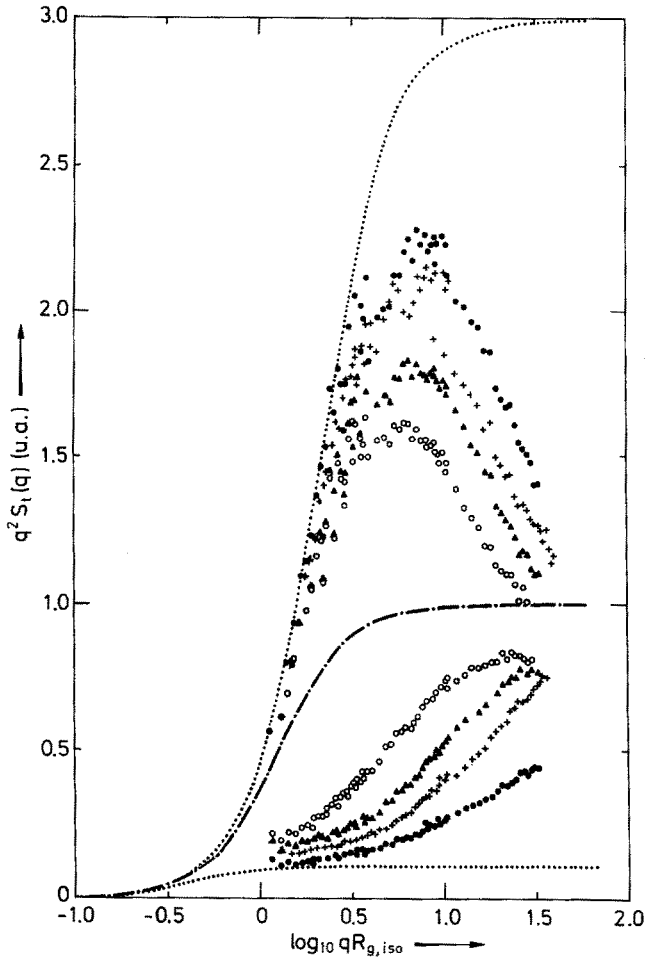

Fig. 3. Data for the single chain from factor $S_t(q)$ in $q^2S_t(q)$. Representation against log $qR_{g\,iso}$ for the following sample of set I: ●, 71 (t^{117} = 10 s); +, 18 (t^{117} = 60 s); ▲, 49 (9000 s); and ○, 50 (130000 s), Dashed dotted line is for the isotropic Gaussian conformation and dotted lines for the completely affine deformation of that latter in parallel and perpendicular direction

deformations in polymer materials: the system of chains causes a reduction in deformation from a macroscopic down to a quasinil deformation of the chemical bond. This can be called a loss of affineness in reference to the totally affine deformation, where it is assumed that the deformation remains the same down to the monomer (which is unrealistic). Two remarks on this concept of loss of affineness are necessary. First, when the deformation is totally recoverable, one expects a threshold in length above which the deformation is affine to the one imposed macroscopically. This corresponds to t/T_{max} sufficiently small. T_{max} is the maximum relaxation time of the system (for a network, $T_{max} = \infty$). At longer t, the deformation will relax even at the macroscopic level. But it is expected that the remaining deformation will still decrease when the scale decreases. Second, the scale of onset of the loss of affineness

is not obviously the global size of the chains or smaller, but could rather be of a much *larger* scale. In that latter case the form factor is blind for distances larger than R_g, and and for $qR_g \ll 1$ always exhibits the deformation for any q. The unique way to explore larger distances is to increase the molecular weight of the chain.

Figure 3 also shows that, when the time increases, the form factor is less and less oriented, so that for $t = \infty$ the chain would be isotropic for any scale. We here consider the different ways of characterising the decreasing of orientation together with the decay of orientation with time.

3.2 Orders of Magnitude of Times. Difficulty of Estimation

To determine the required time range, it is necessary to first compare the classically obtained times from the viscoelastic behaviour (Fig. 1). The situation is complicated by the fact that these times depend on the temperature. The usual glass time temperature superposition (see Sect. 2) has been checked in the 50s for rheological data: the characteristic times τ_{tr}, T_{ter}, etc. depend on the temperature [12] T by the same factor $a(t) = 10(c_1(T - T_g)/c_2 + T - T_g)$. For the SANS data, a similar superposition has been proposed [20]: a form factor for $t = t_1$ at T_1 is compared to a form factor for $t_2 = (a_{T_1}/a_{T_2})t_1$ at T_2. A satisfying overlapping is possible by a correct choice of c_1, c_2 and T_g (see Fig. 4). A similar superposition was found in inelastic measurements for large q [21]. Unfortunately, an important uncertainty remains when choosing c_1, c_2 and T_g. For viscoelastic measurements the values differ [12]; one reason is that experiments using frequency measurements were more conveniently carried out at high temperatures for very liquid melts. Data from Ref. [12] and, more recent, from Ref. [22] have been compiled in Ref. [20] for:

— the Rouse time of large chains of molecular weight M. For this purpose we took the maximum time of a small chain (M′) inside the range of mass where the Rouse model appears valid, $T_{ter} \propto M'^2$, and multiplied by $(M/M')^2$. Among these Rouse times is the one for a chain of mass M_e, the mass between entanglements. We used an estimate of τ_{tr}, as classically admitted [12].

— the terminal time T_{ter} for large molecular weights. For this purpose we used different laws $T_{ter} \propto M^\alpha$ where α is between 3.0 and 3.8.

The obtained values are given in Table 1. These values will be used throughout this paper with a standard temperature of 117 °C; any time at any temperature can be given also in equivalent time at 117 °C, noted t^{117} (see Table I). Another source of error is the extrapolation of the molecular weight: the polydispersity is imprecisely described for some data, and its effect is still uncompletely known. It seems best to measure the characteristic viscoelastic times by measuring the stress in our stepstrain experiment, as was done for the data of set I[20] and II (see Table 1).

3.3 Evolution with Time and Parallel to the Viscoelastic Modulus G(t)

The data of set I, which are the most complete for the considered time range (representative data of Fig. 3), are now used for a qualitative description of the variation with time. In the initial range, the radius of gyration R_{gper} does not change; the relaxation

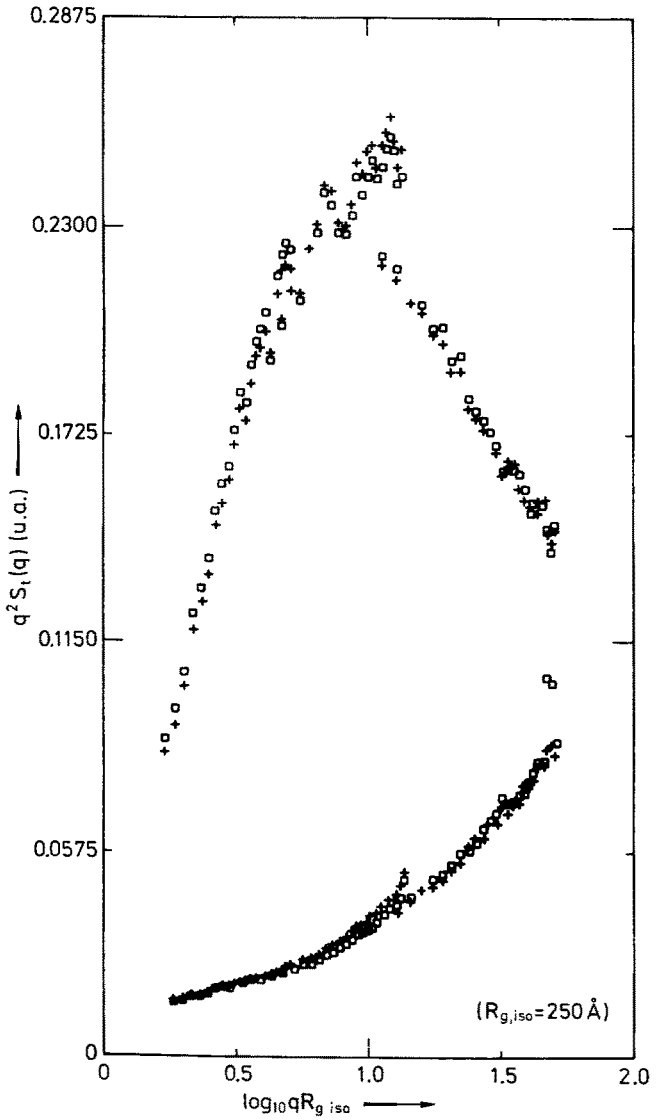

Fig. 4. Agreement with the time temperature superposition for two samples stretched and relaxed at different temperatures in order to have same reduced time $t^{117} = 60$ s. +, 18, T = 117 °C; □, 24, T = 124 °C

occurs, in the perpendicular direction only at large q, and in the parallel direction for all values of q, but is much faster at large q. In the second regime, the radius of gyration starts to change; the relaxation occurs at any q; in the perpendicular, the height of the maximum decreases, and in the parallel direction, the curve increases for all values of q; however, the relaxation at large q is notably slower than before. This can be characterised in terms of the decay time τ as a function of q; for the initial time

Table 1.

Set	Masses	$T_{ter}^{117}(M_{wD})$	T	t	t^{117}	q range	Ref.
I Stretched $\lambda = 3$	$M_{wD} = 780000$ $M_{nD} = 555000$ $M_{wH} = 760000$ $M_{nH} = 660000$	$5 \cdot 10^5$–$5 \cdot 10^6$	113 117 122 128 134	30 s 30 s to 20 mn 30 s to 20 mn 1 mn to 30 mn 1 mn, 16 mn	6 s 30 s–1200 s 200 s–$8 \cdot 10^3$ s $2 \cdot 10^3$ s–$6 \cdot 10^4$ s 10^4 s, $1.3 \cdot 10^5$ s	($Å^{-1}$) $7 \cdot 10^{-3}$, $2 \cdot 10^{-1}$.	9) 10) 20)
II Stretched $\lambda = 3$	$M_{wD} = 95500$ $M_{nD} = 81400$ $M_{wH} = 117000$ $M_{nH} = 105000$	$5 \cdot 10^3$ s	113 117 122	10 s to 10 mn 30 s to 20 mn 30 s to 20 mn	2 s–120 s 30 s–1200 s 200 s–$8 \cdot 10^3$ s	idem	9) 10)
III Stretched $\lambda = 3$	$M_{wD} = 95500$ $M_{nD} = 81400$ $M_{wH} = 1600000$ $M_{nH} = 1300000$	$5 \cdot 10^3$ s	same as II			idem	9) 10)
IV Stretched $\lambda = 3$	$M_{wD} = 31900$ $M_{nD} = 28500$ $M_{wH} = 1600000$ $M_{nH} = 1300000$	100 s	113	30 s to 20 mn	6 s to 240 s	idem	9)
V Shear $\gamma = 4$	$M_{wD} = 780000$ $M_{nD} = 555000$ $M_{wH} = 760000$ $M_{nH} = 660000$	$5 \cdot 10^5$–$5 \cdot 10^6$ s	117 122 128	1 mn 1 mn to 20 mn 10 mn	60 s 400 s–$8 \cdot 10^3$ s $2 \cdot 10^4$ s	$7 \cdot 10^{-3}$, 10^{-1}.	28)
VI Stretched $\lambda = 4.6$	$M_{wD} = 2.6 \cdot 10^6$ $M_{nD} = 2.1 \cdot 10^6$ $M_{wH} = 1600000$ $M_{nH} = 1300000$	$5 \cdot 10^6$–$5 \cdot 10^7$ s	116 150	1 mn 1 mn, 10 mn 30 mn, 40 mn	60 s $3 \cdot 10^4$ s, $3 \cdot 10^5$ s $1.2 \cdot 10^6$ s	$7 \cdot 10^{-3}$, $6 \cdot 10^{-2}$	29)
VII	$M_{wD} = 400000$	$4 \cdot 10^4$–$4 \cdot 10^5$ s for each blend:					
Stretched $\lambda = 4$	$M_{wH} = 200000$ 400000 760000 1600000		122 128	1 mn 1 mn	400 s $2 \cdot 10^3$ s	$7 \cdot 10^{-3}$, $6 \cdot 10^{-2}$.	48)
VIII Rubber γ crosslinked Matrix 1600000 Labeled path of mass $2.6 \cdot 10^6 = M_{wD}$ Stretched $\lambda = 4.6$		$T_{ter} = \infty$	116 150 150	10 s 1 mn 30 mn	10 s $3 \cdot 10^4$ s $9 \cdot 10^5$ s	 $7 \cdot 10^{-3}$, $6 \cdot 10^{-2}$.	31)

range it follows that $t > \text{or} \sim \tau(q)$ for $q > 1/R_g$ and $t \ll \tau(q < 1/R_g)$; for the second range we have $t \sim \tau(q)$, while $\tau(q)$ varies with q. In a third range, the data for large q are already very close to the isotropic value; the relaxation does not seem faster at large q than at small q. An inflexion point appears in both the parallel and perpendicular curves.

This behaviour will be explained in the following sections. Here a qualitative comparison with the variation of G(t) is made. In Fig. 1 three behaviours also appear for G(t), corresponding to the transition zone ($t < \tau_{tr}$), the plateau regime ($\tau_{tr} < t < T_{ter}$), and the terminal region ($t \sim T_{ter}$). Using a time-temperature superposition at 117 °C for $M_{wD} = 7 \cdot 10^5$ yields: $\tau_{tr} \sim 10$ s, $T_{ter}/10 \sim 5 \cdot 10^4$ s, and $T_{ter} \sim 5 \cdot 10^5$ s. These values may agree with the boundary values for the three time ranges of $S_t(q)$. Similar comparisons are also made below for other masses.

3.4 The Opposite Point of View of the Radius of Gyration and of the Intermediate Regime

Particularly in the polymer field, experiments have been mostly, and often very schematically, divided into two categories: studies of the global size of a chain, and measurement of the radius of gyration R_g, or studies of the inside of the chain, then considered to be infinite and with a behaviour f(q). R_g is easily measured, tabulated and compared, while f(q) can be difficult to interpret, unless a simple variation is predicted, as certain scaling concepts in polymer physics, which may lead to a power law as $f(q) \propto 1/q^{\delta}$.

The regime in which to study the global size corresponds to $qR_g \ll 1$ and is called the Guinier regime. In practice, allowing certain approximations, this can be extended to $qR_g < 2$ for a quasi-Gaussian chain. The regime of the inside of the chain, as it is infinite, corresponds to $qR_g \gg 1$ and is called the intermediate (or assymptotic) regime. In practice, for a quasi-Gaussian chain it starts at $qR_g = 5$ and is limited at high q by the size of the statistical unit b (see Sect. 13; $b \sim 12$ Å for PS).

Difficulties in quantifying the form factor. One difficulty of SANS is apparent: the q range is not a large as hoped for! For a radius of 200 Å, q will be at the extreme edge of the Guinier regime, while the molecular weight of the chain is not as large ($5 \cdot 10^5$ for PS melt). For a radius of 100 Å, the intermediate regime starts at $q \sim 5 \cdot 10^{-2}$ Å^{-1}, but is narrow as $1/b \sim 10^{-1}$ Å^{-1}. In the case of deformed melts, the complication is that the different boundaries vary with the direction φ of q with the stretching axis. Also, as the chain is not really Gaussian, their relation with R_g could be slightly different.

For those reasons the use of a calculated form factor derived from models and their comparison to the whole experimental form factor is an alternative to interpretating the data with different advantages and incoveniences. In the following sections we will thus use the three approaches: radius of gyration, intermediate regime, and calculated form factors.

4 Review of Neutron Investigations on Stepstrain Deformation

A first set of data was obtained by the CRM Saclay group in a range of rather large q from 10^{-2} Å^{-1} to $5 \cdot 10^{-1}$ Å^{-1} [23]. Only the effect of a weak deformation ratio λ (1 to 1.7) was observed, without taking into account the effect of other important parameters such as temperature of stretching, speed of deformation, duration of stretching, and quenching. No loss of anisotropy with increasing q was found, arising from the combination of the small values for λ, the narrow domain for q, and the rather large uncertainty. Thus it was possible to fit a totally affine deformation (see definition below). Values for larger λ (2, 3.5, and 5) are also given in Ref. [23] where the temperature assumed three different values for $\lambda = 3.5$. These data were analysed in the parallel direction in terms of a one-dimensional rubber elasticity model of deformation, where the mesh size was taken as an adjustable parameter depending on the temperature. The results were not systematic, mainly because of inefficient substraction of incoherent background values, consecutively to low fractions of deuterated chains, and low flux of the spectrometer.

A systematic variation of S(q) with the different parameters was obtained [24] with λ as 2, 3, and 4.5 and T as 115 °C, 120 °C, 130 °C, and 140 °C. The molecular weight of the chains was monodisperse before moulding and ranged around 150000. A simplified model of rubber elasticity was again used; within this frame the data provided a systematic variation, assuming that molecular weight of the mesh — i.e. the part of chain between two consecutive crosslinks —, depends on the temperature. As no dynamics was included in the model, this mesh molecular weight had also to be time-dependent. A proposal to assimilate the melt to a temporary rubber in the so-called plateau regime will be discussed below. This regime, for which the mesh size is expected to be constant with time and very weakly dependent on temperature, was not explored by the first experiments, both because of too short times and too short chains.

Another published preliminary experiment was performed by the Imperial College group [25]. The obtained qualitative results were in agreement with the results of Ref. [23].

The most complete set of data, referred to below, is a thesis [9] published only in part [10, 20, 26]. Four mixtures with different molecular weights were used (set I, II, III, and IV of Table 1). The q range was wide, as various settings of spectrometers were used (at ILL, Grenoble); q ranged from $5 \cdot 10^{-3}$ Å^{-1} to $3 \cdot 10^{-1}$ Å^{-1}. Set I had the largest molecular weight ($M_{wD} = 7 \cdot 10^5 \sim M_{wH}$) over a wide range of time and temperature. Using the time-temperature superposition covers four and a half decades. The elongation ratio was mainly 3, while 2 and 1.5 have been used.

Other authors [27] published interesting results on the radius of gyration for coextruded samples; polystyrene of relatively high mass ($M_{wD} = M_{wH} = 6 \cdot 10^5$) was used. A strip of polystyrene was inserted into a cylindrical billet of polyethylene, extruded at T = 127 °C at a pressure of 280 kg/cm^2 and with a deformation rate of 0.1–0.2 cm/mn. The deformation ratio, measured from marks on the sample, attained very large values: $\lambda = 3$, 4, 5, and 10. It is difficult to give a corresponding value of t for this deformation, but an indication is that the recovering was tested as total. The results, obtained only from a comparison to the affine behaviour, are presented in Sect. 5.

In addition to sets I–IV, we performed experiments on a different type of deformation (shear [28]) (set V)) and recently on higher molecular weights (set VI). For the latter we also studied the same mixtures but crosslinked (set VIII); this creates long labeled paths of high molecular weights linked to the network by numerous junctions and allows to compare rubbers and melts [29,49] (Sect. 10). Finally, some studies on the effect of the molecular weight of the host chains, i.e. the matrix, were also performed; earlier, the four possible pair-combinations of molecular weights $1 \cdot 10^5$ and $6 \cdot 10^5$ (see Table 1) were compared [30]. More recently, we have investigated the relaxation of a labeled chain ($4 \cdot 10^5$) solved in four different matrices ($2 \cdot 10^5$, $4 \cdot 10^5$, $7 \cdot 10^5$, $1.3 \cdot 10^6$, set VII) [31]. Preliminary results exist also on the interesting case of high-molecular-weight specimens ($1.3 \cdot 10^6$) within a low-molecular-weight matrix (10^5) [32], for which the effect of the concentration of large chains was also studied [32].

5 Quantitative Behaviour of a Finite Chain: Radius of Gyration

Usually SANS does not provide a q range such that $qR_g \ll 1$, except for very small chains. Measurements at $q < 10^{-3}$ Å^{-1} are delicate and consume enormous beamtime. Measurements reported here are only for $0.5 < qR_g < 2$; the extraction of R_g in this range involves assumptions on the chain conformation (i.e. it was considered as Gaussian at large distances) and a careful use of the different methods (e.g. the Zimm plot and other plots which fit the Debye function, see Refs. [9] and [33]). It is actually not possible to measure the parallel radius for large extensions except in the case of rather small chains (as $M_{wD} = 32000$, see below). For $M_{wD} \sim 100000$, we give an "apparent" parallel radius. For chains of $M_{wD} \sim 600000$, this is no longer possible, except for a special extrapolation in the case of affine behaviour in all directions φ (see last part of Sect. 5.1).

5.1 Short Time Behaviour. Comparison to Affine Values

From early investigations it appeared natural to compare the measured value of R_g with the affine value:

$$R_{gx} = \lambda_x R_{g\,iso} \tag{5.1}$$

where x is a Cartesian coordinate of one principle axis of deformation. It occured that the earliest data checked grossly Eq. (5.1) for the following reasons: a streching at T between 115 °C and 130 °C followed by a fast air quenching, corresponding to $10\text{ s} < t^{1/17} < 300$ s, is possible for polymers of molecular weights of $M \sim 100000$ to 150000, which classically are obtained easily by anionic polymerisation. Equation (5.1) is, in fact, not perfectly obeyed for $R_{g//}$ as for R_{gper} (in Ref. [23]) where $\lambda = 1.1$ to 1.7 ($M_{wD} = 1.2 \cdot 10^5$, $M_w/M_n = 1.1$, $(M/M_e) = 6$; the rapid stretching/quenching at T = 102 °C gives $t^{1/17} \sim 50$ to 100 s). The discrepancy is around 10 %, but the measurement of the macroscopic deformation λ is not accurate. A similar slight discrepancy appears in the data of Ref. [25] for equivalent $t^{1/17}$ and slightly larger M_{wD} ($1.4 \cdot 10^5$, but $M_w/M_n = 1.7$): $R_{g//}/R_{g\,iso} = 1.74$, $\lambda_{//} = 1.9$, but the uncertainty is larger than

10%. Better controlled data [24] show a better agreement for elongation at constant speed gradients, $s = 0.2\ s^{-1}$, and T = 115 to 130 °C (corresponding to $t^{117} \sim 10$ to 1000 s); we recall that the molecular weight $1.4 \cdot 10^5$ corresponds to the appearance of a plateau behaviour in the viscoelastic data.

More systematic data [9] allow to check Eq. (5.1) with three different molecular weights: $M_{wD} = 3 \cdot 10^4$, 10^5, and $7 \cdot 10^5$ (Table 1). For $3 \cdot 10^4$, even at the shortest time ($t \sim 5$ s), $R_{g\,per}$ as well as $R_{g//}$ (here measurable) are far from the affine value; for $M_{wD} = 10^5$, one obtains $R_{g\,per} = 60$ Å instead of $R_{g\,aff} = 90/\sqrt{3}$ Å; this corresponds to a slight relaxation: assuming a reptation model, it could be a relaxation up to about the tube size which could influence the global size in this range of molecular weight still small ($M/M_e = 5$) [9]. Finally, for a larger value $7 \cdot 10^5$, $R_{g\,per}$ was measured for three values of $\lambda = 1.5$, 2, and 3, and was found to be *precisely affine* [20]; Fig. 5 shows that it remains so for $7\ s < t < 200$ s. In the parallel direction one can see from Fig. 3 (sample 71, t = 7 s) that the form factor, though not in the Guinier range, is close to the affine calculated one; from this we deduced that the parallel radius of gyration of that sample is most probably affine. For this molecular weight, M/M_e is now 30.

Another elegant test of the affineness was carried out by Hadzioannou et al. [27], as described in Sect. 4. As the deformation and coextrusion are different, the value of t is difficult to evaluate. M_{wD} and M_{wH} are similar, at around $6 \cdot 10^5$; thus, only the perpendicular or isotropic radius can be obtained (using, in principle, the same corrections as suggested above). Within the uncertainty, Eq. (5.1) is very well obeyed for $R_{g\,per}$. The parallel radius cannot be measured, but as the isointensity curves appear as ellipses with an affine ratio $(\lambda/\sqrt{\lambda})$, a kind of extrapolation is made along these ellipses, which leads to an affine value for $R_{g//}$. A similar approach, applied to results of set I, permits also to check Eq. (5.1) in the parallel direction for the shortest times.

5.2 Variation of the Radius of Gyration with Time

Figure 5 shows the variation of $(R_g^2/R_{g\,iso}^2)$-1 with log (t) for the data sets I–IV. At short t the value is affine (I) or close to affine (II, III) as seen before; it then changes as times increase in a monotonous way back to 0, the equilibrium value. The speed of decay depends strongly on the molecular weight of the labelled chain. In a sample of $M_{wD} = 95000$ in matrices of $M_{wH} = 105000$ and 1600000, the effect of the matrix appeared weak, except maybe for the longest time (see Sect. 12). For a mixture with $M_{wD} = 32000$ in $M_{wH} = 1600000$ giving close to isotropic values for the longest time, it seems possible to use longer times than those applied here, to obtain a complete relaxation of R_g.

These variations are now used to extract two important behaviours:

The Lack of Contraction

The variation of R_g with time can be an important key test of the tube models if the chains are large enough, as in Ref. [9, 10]. The reason is that not only the complete variation of $R_g(t)$ is predicted by the Doi-Edwards model, but that it also predicts an effect of the tube, called contraction [4] (see Sect. 2.2). The contraction inside the tube leads to an important consequence: the radius of gyration will be reduced by the contraction

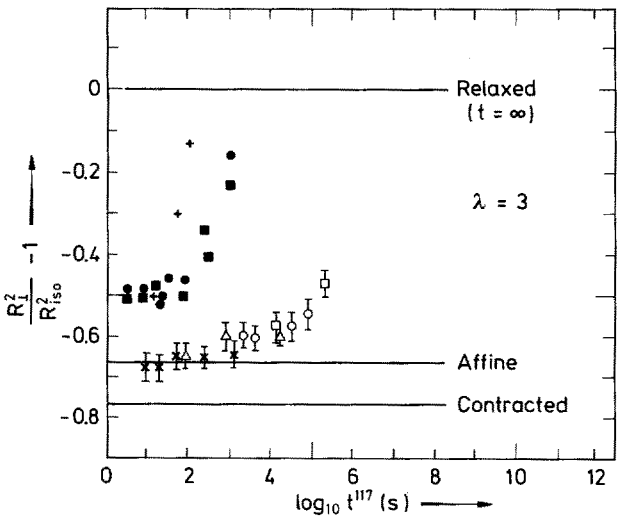

Fig. 5. Relaxation of the transverse radius of gyration after a stepstrain of elongation ratio 3. +, set IV ($35000_D/1600000_H$); ●, set II ($105000_D/95000_H$); ■, set III ($105000_d/1600000_H$); ×, △, ○, □, set I ($780000_D/760000_H$) at temperatures 117 °C, 122 °C, 126 °C, and 134 °C

factor [4] *in the parallel as in the perpendicular* direction. For the perpendicular case, as $R_{g\,per}$ is smaller than $R_{g\,iso}$, the relaxation process of contraction leads to a value even further from the equilibrium value, and the function $R_{gper}(t)$ exhibits a minimum.

A discrepancy between the data for the molecular weight $7 \cdot 10^5$ (set I), in Fig. 6a, is clearly shown in Ref. [20]. The data for $R_{g\,per}$, as previously mentioned, are monotonously increasing without any minimum. The calculated curves are for the ratio $T_{eq}/T_{dis} = 10^{-1}$ and 10^{-2}; for a mass M it is theoretically equal to $6M/M_e > 10^2$,

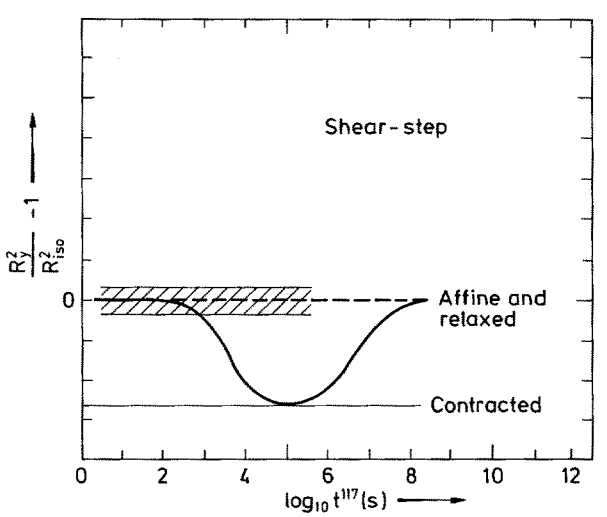

Fig. 6. Relaxation of the radius of gyration in a step-shear experiment: solid line predicted (DE model); dotted line, experimental (////)

and M is surely more than $5 \cdot 10^5$. The polydispersity certainly has to be taken into account ($M_w/M_n = 1.4$), but simple evaluations imply that this would not suffice to mix the two processes of equilibration and disengagement enough to cancel the effect.

The variation of $R_g(t)$ for small masses also does not show any contraction in Fig. 5. But in that case the molecular weights are too small for a conclusive test.

To increase the efficiency of the test, two complementary experiments were performed in collaboration with Osaki. The first [28] uses the same molecular weight ($7 \cdot 10^5$, set V), but a different deformation, namely shear instead of extension (see Sect. 2). In the case of shear there is one direction for which the macroscopic deformation ratio is $\lambda_y = 1$. Thus, the affine value of R_{gy} is equal to $R_{g\,iso}$; the contraction would again lead to a decrease and the disengagement would cause a return back to $R_{g\,iso}$ (Fig. 6). Such a variation could allow a more precise check. The results are the following: for short times ($t^{1/7} \sim 30$ s to 1000 s) R_{gy} is equal to $R_{g\,iso}$, as expected. For longer times a minimum is not observed and R_g always remains constant. The second complementary experiment uses uniaxial stretching but for much larger molecular weights (set VI, $M_{wD} = 2.6 \cdot 10^6$, $M_{wD}/M_{nD} = 1.15$ before moulding, and $M_{wD} \sim 2 \cdot 10^6$, $M_{wD}/M_{wH} = 1.5$ after moulding) with a larger stretching ratio, $\lambda = 4.6$, which enhances the theoretical contraction factor. Data are available only up to t = 40 mn at 140 °C, and thus approx. $t^{1/7} = 8 \cdot 10^5$. The Rouse time $T_{eq} = T_{Rouse}$ is estimated between 10^4 and $4 \cdot 10^5$ (Note 1). Thus, the contraction would be visible. On the contrary, $R_{gy\,per}$ increases monotonously with t.

Note 1: The Rouse time can be estimated: (i) from the value of T_{ter} (estimated in Ref. (13)), divided by $6M/M_e$, i.e. $5 \cdot 10^6/6 \times 100 \simeq 10^4$, (ii) from the estimated Rouse time (JPhys82) for $M = 7 \cdot 10^5$, multiplied by $(2 \cdot 10^6/7 \cdot 10^5)^2$: a first set of estimations 15000 to 50000 for $7 \cdot 10^5$ gives here 10^5 to $4 \cdot 10^5$. A second, much lower estimate of ~ 3000 gives $2 \cdot 10^4$.

Terminal Time of the Radius of Gyration

Apart from the contraction effect, described above, it is difficult to determine differences between the Rouse model and the reptation model via the time variation of R_g. The predicted variations are:

$$R^2_{g\,Rouse}/R^2_{g\,iso} - 1 = \sum_{all\,p} 1/p^2 \exp(-p^2 t/T_{Rouse})$$

$$R^2_{g\,rep}/R^2_{g\,iso} - 1 = \sum_{p\,odd} 1/p^4 \exp(-p^2 t/T_{dis})$$

These are slightly different at short time, i.e. in a range $t/T_{dis} < 10^{-2}$; but unless the chain is extemely large, this is the range where other processes are involved. At long t ($t/T_{dis} > 10^{-1}$), the decay is close to exponential for both models. Figure 7, plotting $\log(R^2_g/R^2_g - 1)$ versus t displays a fast relaxation at short t; for the case of set I ($M_{wD} = 7 \cdot 10^5$) this corresponds to the relaxation observable in Fig. 5 occurring in the time range of equilibration but in the opposite direction. Only the points at long t give a straight line, the slope of which gives the terminal decay. We must stress that the weakness of this extrapolation is the too short times used compared to the obtained terminal time. These will be compared to the terminal time in the relaxation of the stress.

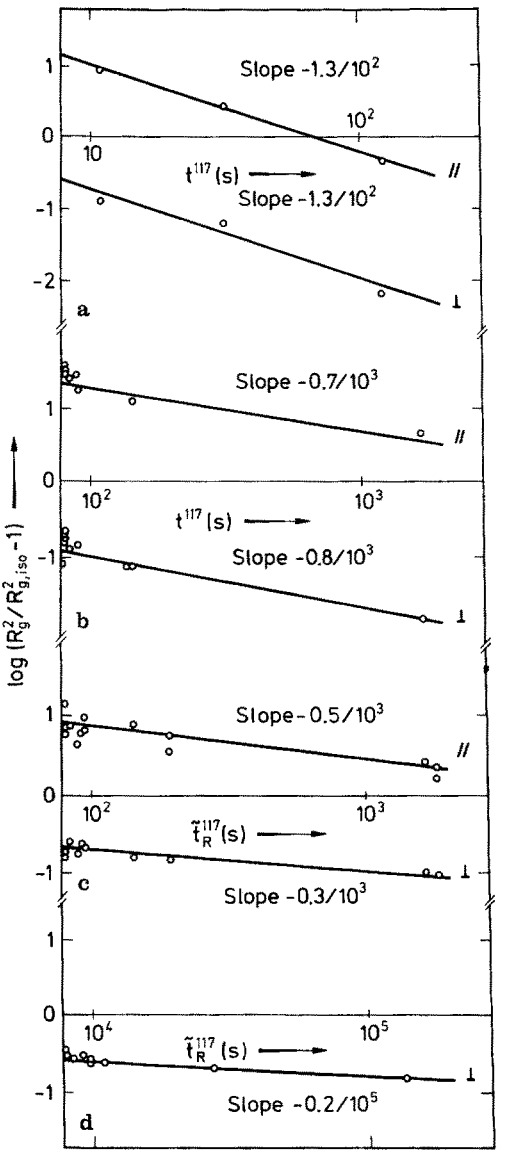

Fig. 7a–d. Relaxation of radius of gyration for set IV (**a**), II (**b**), III (**c**), and I (**d**) with time in log-lin representation

In the case of the molecular weight $7 \cdot 10^5$ (set I) we measured the decay of the stress for different samples during their preparation, and used the time-temperature superposition to obtain a mastercurve [20]. By comparing the results with data from Tobolsky [34], a terminal time of $T_{dis} = 5 \cdot 10^5$ s was obtained. This is within estimations based on the extrapolation of other data of the latter author ($5 \cdot 10^5$ s $< T_{ter} < 2 \cdot 10^6$ s). The terminal time value for R_g is $T_{ter} = 5 \cdot 10^5$ s, which is equal to the value of the stress. For set II and III, an similar value was found for the perpendicular and the apparent parallel radius. Thus, $1.5 \cdot 10^3$ s for the matrix $M_{wH} = 105000$ and $3 \cdot 10^3$ s

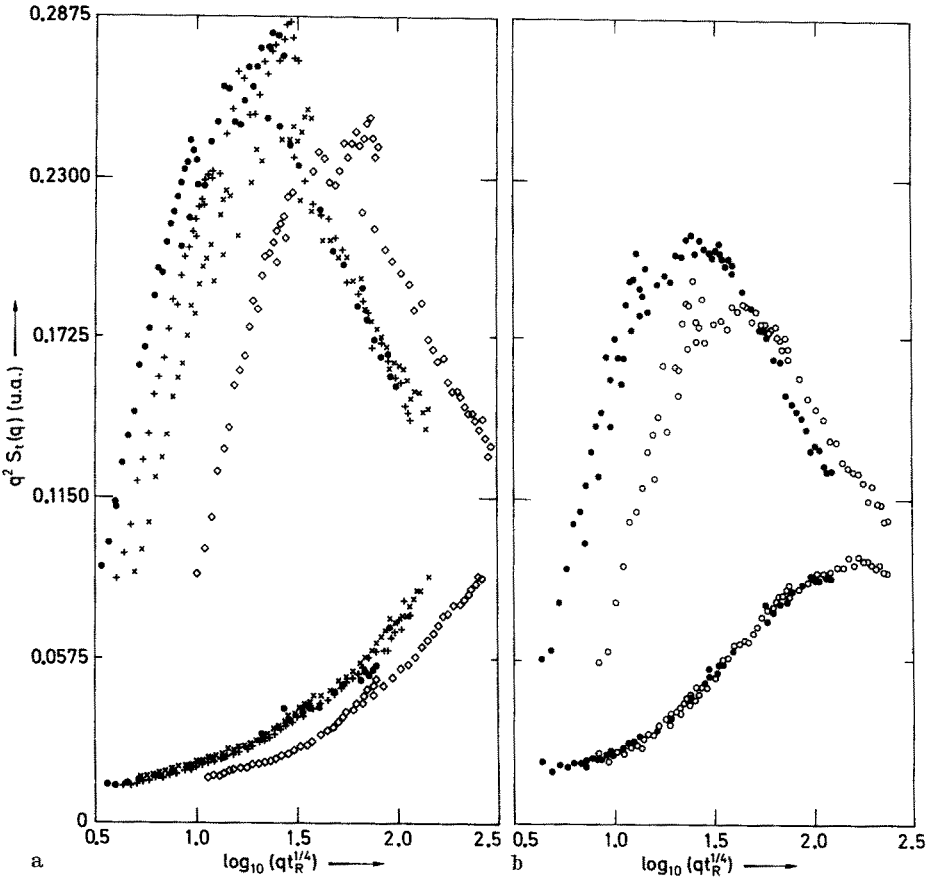

Fig. 8a. Test of a $qt^{1/4}$ using horizontal shift in $\{q^2S_t(q), \log qR_{giso}\}$ representation for short times, t^{117} = 10 s, 20 s, 60 s, and 240 s; **b** Same for long times 9000 s and 130000 s

for M_{wH} = 1600000. Table 1 gives $T_{ter} = 3 \cdot 10^3$ s. Finally the value for M_{wD} = 32000, from the perpendicular and parallel radius, is 70 s. Table 1 gives (from multiplying T_{Rouse} for $7 \cdot 10^5$ by $(32000/710^5)^2$) 30 s to 100 s, i.e. again a very good agreement.

5.3 Summary

SANS appears to be the only method to provide the time variation of a chain's global size in a melt, and this leads to three important observations:

— the radius of gyration is affine at short times, for large enough chains; the shorter the chain, the faster the departure from the affine value.

— at intermediate times, the relaxation of the radius is visible, and is in the opposite direction to the contraction predicted by the Doi-Edwards model.

— at longer times, the value of the radius terminal time is equal to the stress terminal time, obtained either from measurements during samples preparation or from estimations based on literature data, the comparison remaining unprecise.

6 Simple Asymptotic Laws for an Infinite Chain. The Intermediate Regime

For an isotropic melt, the single chain form factor can be fitted by the Debye function over the q range $5 \cdot 10^{-3}$, 10^{-1} Å^{-1}. At large q it is close to:

$$S(q) \propto \frac{1}{q^2a^2 + 1/M} \propto 1/q^2a^2 \qquad (M\infty) \tag{6.1a}$$

with

$$q \gg 1/R_g \tag{6.1b}$$

which can be called the asymptotic law for a Gaussian chain. M tends towards infinity, and a is equivalent to the size of the lattice cell: then, no other physical characteristic size is involved in the problem, as in the scaling laws of critical phenomena at the critical temperature T_c ($T - T_c = 0$ corresponds here to $1/M = 0$). Experimentally, Eq. (6.1) must be checked for $qR_g \gg 1$; in practice, $qR_g > 5$ is satisfactory. Pioneer tests [35] were on $M_w = 10^4$ to 10^5; during our experiments we checked Eq. (6.1) for $M_w = 7 \cdot 10^5$ and $2.6 \cdot 10^6$ (with a careful annealing of the sample). We describe in Section 14 how Eq. (6.1a) should appear not valid at large q, where the persistence length is involved.

What could be an asymptotic law for a deformed chain? Only three asymptotic laws are known; these correspond to classical models not explicitly involving any size or time parameter.

6.1 Totally Affine Deformation

This model is static, since time is not involved; it assumes:

$$\underline{r} \to \tilde{\tilde{E}}\underline{r} \tag{6.2}$$

where $\tilde{\tilde{E}}$ is the deformation tensor. In that case Eq. (6.1) becomes via Eq. (6.2):

$$S_{aff}(q) = 1/(\lambda_q^2 q^2) \tag{6.3}$$

where $\lambda_q^2 = \langle q \cdot \tilde{\tilde{E}} \cdot q \rangle / q^2$. To confirm this law one simply must plot $q^2S(q)$ versus any function of q; which must give a plateau. This is represented in Fig. 3 by the dotted curves for the perpendicular and parallel directions. Most of the data do not fit these curves in the region of q where they display the plateau. In the perpendicular direction, they overlap at $S_{aff}(q)$ only at short t and for small $qR_{g\,per}$, ~ 1, not in the asymptotic regime. For very long chains, this q range would correspond to $qR_{g\,per} > 5$ ($M \sim 10^7$), such that it is expectable that at equally short t, Eq. 6.3 would hold in the asymptotic regime. In parallel direction the overlap exists only for the shorter t and the smallest q values; this is nearer on more recent data on large

molecular weight ($M_w \sim 2 \cdot 10^6$); in these case, we are in the asymptotic regime, as $qR_{g\,par} \gtrsim 5$.

6.2 The Rouse Superposition Law

Using the complete calculation (given in Sect. 7), and including the conditions of Eq. (7.10a),

$$qR_g > 3\,, \qquad t \gg \tau\,, \qquad t \ll T_{Rouse}\,, \qquad q\varrho \ll 1\,,$$

where ϱ is the size of the Rouse subchain, leads to [36]:

$$S(q) = 1/q^2 f(qt^{1/4}) \tag{6.4}$$

where f depends on λ and the direction of q with the deformation axes, but does not explicitly involve any size or time.

We do not clearly know ϱ, i.e. the Rouse subchain size, neither the elementary hopping time τ_N. But the two of them are related by the same relation than the radius of gyration and the maximum Rouse time, both measured quantities:

$$\frac{\tau_N}{\varrho_4} = \frac{T_{Rouse}}{R_g^4} = \text{cst.}$$

Taking ϱ equal to the persistence length, $\varrho = b = 12$ Å, $\tau_N \sim 10^{-2}$ s at 117 °C.

The relation between q and t of Eq. (6.4) appears by plotting $q^2S(q)$ as a function of $(qt^{1/4})$. An easy procedure is to use for the abscissa log $(qt^{1/4})$ a large (q, t) range. The superposition of the curves in the range corresponding to Eq. (7.10a) should work for any direction. For the most complete set of data (set I), Fig. 8 shows the accuracy of the test. First, samples relaxed at same temperatures were compared to avoid the uncertainty caused by the time-temperature superposition. The largest uncertainty then results from the form factor, but would not artificially improve the fit in both directions: e.g., if an error reduces the form factor in the perpendicular direction, as would a supplementary relaxation, it would also do so in the parallel direction, which would then appear less relaxed. The result of this fit is:

— within a first time range, the superposition is satisfactory for both parallel and perpendicular directions in the q range between $2 \cdot 10^{-2}$ and $2 \cdot 10^{-1}$ Å^{-1}. This corresponds to Eq. (7.10a).

— within a second time range there is no overlapping neither for the perpendicular nor for the parallel direction.

— within a third time range, of the largest times, the superposition is again surprisingly good in the parallel direction, while it appears unfavorable in the perpendicular.

A slightly different method, using the $q^2S(q)$ representation, is to search for the best superposition by translation of the log (q) abscissa, which gives $\Delta_t \log q$ for each value of t (taking zero for a given t_0). Figure 9 allows to check whether this best superposition agrees with 6.4, i.e. whether $\Delta \log q = 1/4 \log (t/t_0)$. Equation (6.4) is checked

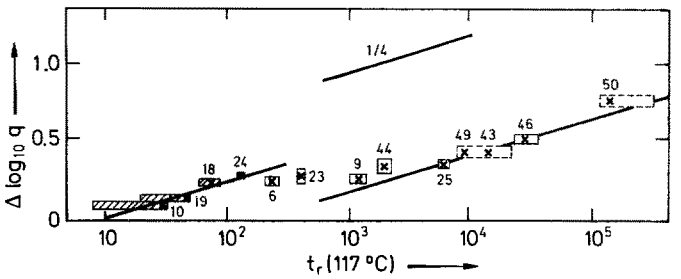

Fig. 9. Values of the horizontal shift Δ log q(t) from superposition as in Fig. 8. Solid lines have the slope 1/4

at short times, where a departure is observed. A second slope 1/4 can be found at longer times.

It seems that the same behaviour on the same time scale also can explain the data for the lower molecular weights (100000 in a matrix of 100000 or 1 600000).

In summary, a ($qt^{1/4}$) superposition is predicted by the Rouse model, and is checked within the uncertainty in the short time region for q large enough. It appears again at long times, but in the parallel direction only.

6.3 Asymptotic Law for the Disengagement Process

The genuine theory of reptation again does not involve any parameter, as it considers larger scales than the size of the tube. That condition is obeyed if

$$q \ll 1/D \tag{6.5}$$

where D is the tube diameter. Only the second and third process are testable. Here we consider only the third, i.e. at time t, chains during their disengagment after an initial deformation, with two ends already disengaged and a centre part still in its "old" tube. If the chain is long enough, it assumes a q range corresponding to the distances:

$$d(q) \ll R_{parts} \tag{6.6}$$

or chemical distances along the chain:

$$n(q) \ll N_{parts} \tag{6.7}$$

where R_{parts} and N_{parts} are the size and the chemical length of either the disengaged or the still engaged parts. Within this q range the interference terms between monomers of different parts is proportional to n(q), while the terms for monomers of the same parts are proportionnal to N_{parts}. Thus, the interference term is not significant and one can simply add the two terms of the engaged (S_{aniso}) and disengaged part (S_{iso}):

$$S_t(q) = \mu(t)S_{aniso}(q) + (1 - \mu(t)S_{iso}(t) \tag{6.8}$$

where $\mu(t)$ is the average fraction of the engaged part (memory function). Assuming a totally affine (contraction factor $c = 1$) or an affine plus contracted ($c > 1$) deformation for $S_{aniso}(q)$, we have:

$$S_{aniso}(q) \sim \left(\frac{c}{\lambda_q^2}\right)\left(\frac{1}{q^2}\right)$$

$$S_t(q) \sim \left(\frac{1}{\lambda_q^{*2}(t)}\right)\left(\frac{1}{q^2}\right)$$

$$1/\lambda_q^{*2}(t) = 1 + \mu(t)\,(c/\lambda_q^2 - 1)\,.$$

In this case there is a kind of uniform relaxation, valid only in Eq. (6.6) (in particular, the decay of the radius of gyration is different at short times; see Sect. 8).
Equation (6.9) is no more verified by the data than is Eq. (6.3) in the short time range which is due to the same reason, the impossibility to simultaneously obey Eqs. (6.5) and (6.1 b). However, Eq. (6.8) is still claimed to be valid, with a different S_{aniso} than the one given by Eq. (6.9). In that case it follows that:

$$S_t(q) - S_{iso}(q) = \mu(t)\,(S_{short\ t}(q) - S_{iso}(q)) \tag{6.10}$$

where $S_{short\ t}$ represents the form factor at the beginning of the disengagement, admitting that the different processes are well separated in time. Then Eq. (6.10) reflects the important feature of reptation, i.e. that small distances are affected by the longer times of the disengagement process which actually involves larger scales much more strongly than for the Rouse model. This was also proposed for the dynamic form factor [35]. For that case we assumed that [26]:

$$\mu(t) \sim \exp(-t/T_{ter}) \tag{6.11}$$

and

$$(\log(S_{t1}(q) - S_{iso}(q)) - \log(S_{t2}(q) - S_{iso}(q)))/(t_1 - t_2) \tag{6.12}$$

was plotted versus q. A plateau at high q was approximately obtained for different combinations of four values of t. Here, the largest values of t ought to be used. A quan-

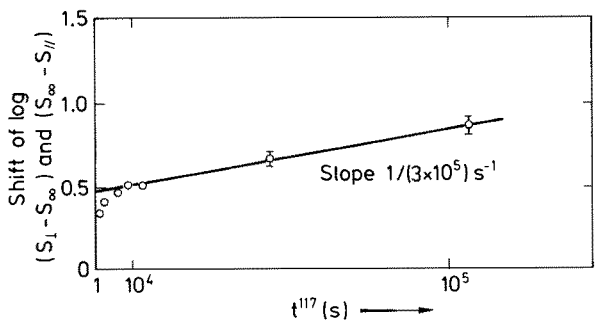

Fig. 10. Variation with time (linear scale) of the shift in $\log(S_t$ per $(q) - S_{t\,iso}(q))$ (resp. $\log(S_{t\,para}(q) - S_{t\,iso}(q))$ allowing best overlapping of theses curves for the different values of t

titative calculation of Eq. (6.10) was given by Noolandi [37] for different pairs of times (t_1, t_2) both shorter or of the same order as T_{dis}, showing that an apparent plateau could be obtained even at small t/T_{ter}.

It is also simple to avoid the assumption of Eq. (6.11). By an alternative procedure we tested an overlapping of the curves $\log (S_t(q) - S_{iso}(q))$ vs. q, at large q, by a simple transition $\Delta_t S$ along the ordinate axis [9, 10, 26]. Figure 10 shows the variation of $\Delta_t S$ with t. The value of the slope obtained from a straight line through the last four points gives $T_{ter\,h.q.} = 3 \cdot 10^5$ at 117 °C. The terminal times for the stress and for the radius of gyration are given in Sect. 5. The agreement between the three times is excellent, although we recall that the uncertainty in this case is very large. There is still a need for experiments at longer t; these are currently pursued.

7 Calculations of Form Factors

Several calculations have been given for the form factor of the chains, after a step-strain of given deformation tensor. These are restricted to a uniaxial deformation (extension to other cases is simple) and to a melt (no solvent): this latter condition allows to admit that, similarly to the isotropic case, the chains behave as Gaussian chains. Then the equality

$$S(\underset{\sim}{q}) = \langle \sum_i \sum_j \exp (i \cdot \underset{\sim}{q} \cdot (\underset{\sim}{r}_i - \underset{\sim}{r}_j)) \rangle = \sum_i \sum_j \exp (-q^2 \langle (\underset{\sim}{r}_i - \underset{\sim}{r}_j)^2 \rangle / 2) \quad (7.1)$$

generally holds for all other cases listed below in this section because all the probability distributions of $(\underset{\sim}{r}_i - \underset{\sim}{r}_j)$ are of the Gaussian type for all models used.

In the case of the Rouse model, the calculation first yields an equation of evolution for $\langle (\underset{\sim}{r}_i - \underset{\sim}{r}_j)^2 \rangle$ (t), then leading to $S_t(q)$. This is similar in the case of the reptation model using the disengagement equation of motion, but this latter concerns only the third process of the Doi-Edwards model; this requires to take into account:

— the second process (contraction), which acts on the entire form factor, but which does not coincide with the data.

— the first process, which acts on a smaller level than the tube diameter D, which is fully attainable in our q range. The description of the state of the system by the Doi-Edwards model is close to that by the rubber elasticity models.

This is one of the reasons for the calculation of a form factor of a deformed rubber at an infinite time after a stepstrain.

7.1 The Rouse Model

The Rouse equation is given by:

$$\zeta \, \partial \underset{\sim}{R}_n / \partial t = \frac{3kT}{\varrho^2} \partial^2 \underset{\sim}{R}_n / \partial n^2 + \underset{\sim}{\varphi}_n \quad (7.2)$$

where ζ is a friction coefficient, n the index of one subchain, $\underset{\sim}{R}_n$ its position, $\underset{\sim}{\varphi}_n$ a random force acting on it, ϱ^2 the mean square length of one subchain, and the boundary conditions are $(\partial \underset{\sim}{R}_n/\partial n)_{n=0} = (\partial \underset{\sim}{R}_n/\partial_n)_{n=N} = 0$. A Fourier transformation gives:

$$\partial \underset{\sim}{X}_p/\partial t = -(3T/\zeta\varrho^2 p^2/N)\, \underset{\sim}{X}_p + \underset{\sim}{\varphi}_p(t) \tag{7.3}$$

solved as:

$$\underset{\sim}{X}_p = \exp(-t/\tau_p) \int_0^t \underset{\sim}{\varphi}_0(t') \exp(-t'/\tau_p)\, dt' + \int_0^N \cos(p\pi n/N)\, \underset{\sim}{R}_n(0)\, dn \,. \tag{7.4}$$

This allows to calculate:

$$\langle(\underset{\sim}{R}_m(t) - \underset{\sim}{R}_n(t))^2\rangle = 2/N \sum_p \sum_q \langle \underset{\sim}{X}_{p\alpha}(t)\, \underset{\sim}{X}_{q\beta}(t)\rangle (\cos(p\pi n/N) - \cos(p\pi m/N))$$
$$\times \{(\cos(q\pi n/N) - \cos(q\pi m/N))\} \tag{7.5}$$

which gives [9], along a given direction α (= x, y, z)

$$\rangle(\underset{\sim}{R}_m(t) - \underset{\sim}{R}_n(t))^2\langle_\alpha = |n - m|\, \varrho^2/3 + \varrho^2/3(A_{\alpha\alpha} - 1) \sum_{p=1}^{N} 2N/p^2\pi^2$$
$$\times (\cos p\pi n/N - \cos p\pi m/N)^2 \{\exp(-t/\tau_p)\} \tag{7.6}$$

with $A_{\alpha\alpha} = \lambda_\alpha^2$ for an initially affine deformation.

Equation (7.6) is directly inserted into Eq. (7.1) to calculate $S_t(q)$ by computer: Refs. [9, 10, 39] give plots in $q^2S(q)$ representation of the results, which are the plain and dotted lines of Fig. 11. An analytic derivation is given by Daoudi [36]. Though convinced to treat a reptation problem the latter author obtained, because of inversion in averaging, the same expression as Eq. (7.6), which can also be written as:

$$\rangle(\underset{\sim}{R}_m(t) - \underset{\sim}{R}_n(t))^2\langle_\alpha = \varrho^2\, |n - m| + \varrho^2(A_{\alpha\alpha} - 1) \sum_{k=n} \sum_{l=n} G_{kl}(2t) \tag{7.7}$$

where:

$$G_{kl}(t) = 2/N \sum_{p=1}^{N} \sin(p\pi k/N) \sin(p\pi l/N)\, e^{-t/c_p} \,. \tag{7.8}$$

This allows exact calculations of an infinite chain, by approximating the function $G_{kl}(t)$ as:

$$G_{kl}(t) = \sqrt{\pi^2/(4t/\tau_N)} \exp(-|k - l|\, \pi^2/4(t/\tau_N)) \,. \tag{7.9}$$

Then $S_t(q)$ can be calculated by identifying the monomer and the subchain, i.e. $\underset{\sim}{r}_n = \underset{\sim}{R}_n$ (valid for $q\varrho < 1$). Using Eq. (7.1), leads, under the conditions: $qR_g > 3$, $t \ll T_{max}$, $t \gg \tau_N$, $N \gg 1$, to:

$$S_t(q) = 1/q^{*2} \int_0^\infty \exp(-(q^2/q^{*2})\, g(x))\, dx \tag{7.10}$$

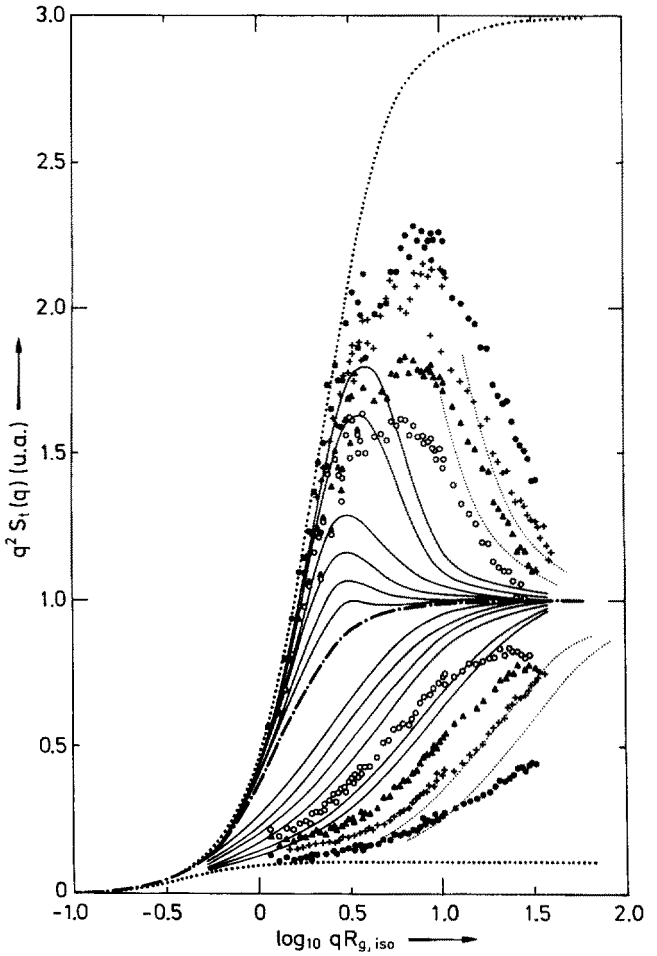

Fig. 11. Calculated form factors for isotropic Gaussian chains (dotted dashed line), completely affine deformation (dotted), Rouse model ($t/T_{Rouse} = 5 \cdot 10^{-5}$, 10^{-4} (tiny dots), $5 \cdot 10^{-3}$, 10^{-2}, $5 \cdot 10^{-2}$, $5 \cdot 10^{-1}$, $2 \cdot 10^{-1}$ and $4 \cdot 10^{-1}$ (solid lines); data as in Fig. 3

or

$$q^2 S_t(q) = (S_t(q)/S_{iso}(q)) = f(q/q^*) = f(qt^{1/4}) \tag{7.11}$$

as $q^* = \pi/\sqrt{8}\,(1/R_g)\,(t/T_{max})^{-1/4}$. This equation shows what was called, in the preceding sections, a (q, t) superposition law. The function f depends on the direction of q with respect to the deformation.

7.2 The Disengagement Model

The calculation outlined here is based on the main process of reptation, i.e. the third process of the Doi-Edwards model, called the disengagement process [9, 39]. The two

first processes are also included in Ref. [39] as the initial conditions for the third process. Therein it is seen that the three processes are well separated in time, which is possible only for long chains. Two averages are designed. The first is a thermal average of all chains with isotropic parts (i.e. already disengaged) from 0 to the linear abcissa along the tube line s_1 and from s_2 to L, but still anisotropic from s_1 to s_2. The distribution of vectors joining two points of the tube line is assumed to be Gaussian. This is obvious for the isotropic part. The anisotropic part of the chain remains under the initial conditions. An affine deformation of the tube line can be chosen. This allows the use of Eq. (7.1) with;

$$\langle(\underset{\sim}{r}_m - \underset{\sim}{r}_n)^2\rangle = \varrho^2/3\,|m-n|\left\{1 - \int_{m\varrho}^{n\varrho}(1 - \lambda_q^2/c)\,H(\sigma - s_1)\,H(s_2 - \sigma)\,d\sigma\right\}$$

where H(x) is the Heavyside function $H(x < 0) = 0$, $H(x > 0) = 1$, and λ_q^2 defined in 6.3 is used to calculate S(q) in a given direction of $\underset{\sim}{q}$.

The second, is an average of the distribution at time t after stepstrain of the pair (s_1, s_2), $p(s_1, s_2, t)$:

$$p(s_1, s_2, t) = (\partial/\partial s_1)\,(\partial/\partial s_2)\,P(s_1, s_2, t)$$

where P is the probability that s_1 and s_2 are contained in the not disengaged part at time t. Noting that $g(s_1, s_2) = S_{s_1 s_2}(q) - S_{iso}(q)$, it follows that:

$$S_t(q) - S_{iso}(q) = \int_0^L dy \int_0^L dx\; g(x, y)\,\frac{\partial}{\partial x}\,\frac{\partial}{\partial y}\,p(x, y)$$

$$= \int_0^L dy \left\{g(x, y)\,\frac{\partial p}{\partial y}(x, y)\right\}_0^y + \int_0^L dy \int_0^L dx\,dx$$

$$\times \frac{\partial g}{\partial x}(x, y)\,\frac{\partial p}{\partial y}(x, y)$$

$$= \int_0^L dy \left\{g(0, y)\,\frac{\partial p}{\partial y}(0, y) - 0\right\} + \int_0^L dy \int_0^L dx$$

$$\times \frac{\partial g}{\partial x}(x, y)\,\frac{\partial p}{\partial y}(x, y)$$

(g(y, y) is equal to zero as it corresponds to one point in the old tube.)

$$= \{g(0, y)\,p(0, y)\}_0^L - \underbrace{\int_0^L dy\; p(0, y)\,\frac{\partial}{\partial y}\,g(0, y)}_{(p(0, y) = 0)}$$

$$\underbrace{+\int_0^L dy \int_0^L dx\, dx \left\{\frac{\partial g}{\partial x}(x, y)\, p(x, y)\right\}_x^L}_{T_2}$$

$$\underbrace{-\int_0^L dy \int_0^L dx\, dx\, p(x, y) \frac{\partial}{\partial x} \frac{\partial}{\partial y} g(x, y)}_{T_1}$$

The derivatives of g(x, y) are calculated, following Eqs. (7.6), (7.14), (7.15) and Vaking $A = \lambda_q^2/c$,

$$T_1(q) = (1 - A)^2 \sum_{p\,odd} (8/\pi^2 p^2 L^2) \int_0^L ds(Q^2 s^3/Q^2 s^2 + p^2\pi^2) \times \exp(-AQ(1 - s)/L) - (p^2 L^2 t/s^2 T_{dis})$$

$$T_2(q) = (1 - A)\, Q(1 + e^{-Q}) \sum_{p\,odd} 8 \exp(-p^2 t/T_{dis})/(p^2\pi^2(Q^2 + p^2\pi^2))$$

with:

$$Q = q^2 R_{g\,iso}^2 .$$

This not really simple algebra can be simplified by physical considerations [39]. First Eq. (7.14) combined with Eq. (7.1) gives the form factor of a isotropic-stretched-isotropic copolymer, which can be directly calculated. The second step then consists in calculating the average S(q) of the copolymer (s_1, s_2) form factors, i.e. $\int p(s_1, s_2, t)\, S(s_1, s_2)\, ds, ds_2$ instead of calculating crudely the form factor of the "average" copolymer ($S(\langle s_1\rangle, \langle s_2\rangle)$). The result is similar at small $qR_g(t)$ and large qRg(t) but slightly different for intermediate values.

At short t, T_1 tends to zero, and $T_2(q)$ to $((1 - A)/6)\, Q\, \Sigma\, (96/\pi^4 p^4) \exp(-t/T_{dis})$, so that:

$$S_t(q) = 1/2\left[1 - \frac{q^2 R_{g\,iso}^2}{3}(1 - (1 - A)\, \Sigma\, (96/\pi^4 p^4) \exp(-p^2 t/T_{dis}))\right] \tag{7.19}$$

which is the Guinier law with the Doi-Edwards expression for the radius of gyration $R_g(t)$ [4].

At large q, $T_1(q)$ tends to $(1 - A)^2/q^2 R_{g\,iso}^2 \mu(t)$ and T_2 to $(1 - a)/Q\mu(t)$ so that finally:

$$S_t(q) = (1/Q)(1 - \mu(t)) + (1/AQ)(\mu(t)) \tag{7.20}$$

with:

$$\mu(t) = \sum_{p\,odd} (1/p^2\pi^2) \exp(-p^2 t/T_{dis}) \tag{7.21}$$

(note that the time function $\mu(t)$ ($\Sigma\ 1/p^2$) is slightly different at short times from $R_g(t)$ ($\Sigma\ 1/p^4$)).

Another elegant derivation of these results was given later by Hong and Noolandi [37]. These authors remarked that an equation of evolution can be derived for the quantity:

$$F_{nm}(t) = \langle e^{i\underset{\sim}{q}\cdot(\underset{\sim}{R}_m(t) - \underset{\sim}{R}_n(t))}\rangle . \tag{7.22}$$

directly from the Langevin equation of the reptation model:

$$\underset{\sim}{R}_n(t + \Delta t) = 1/2(1 + \eta(t))\ \underset{\sim}{R}_{n+1}(t) + 1/2(1 - \eta(t))\ \underset{\sim}{R}_{n-1}(t)$$

which gives:

$$F_{nm}(q, t) = 1/2\{F_{m+1,n+1}(q, t) + F_{m-1,n-1}(q, t)\} . \tag{7.23}$$

The boundary conditions for $R_o(t)$ and $R_N(t)$ give boundary conditions for F_{m0} and $F_{N+1,n}$. Taking the continuous limit of Eq. (7.22) and by Laplace transformation we obtain F_{mn} which can be directly used in $S_t(q) = \Sigma_m \Sigma_n F_{mn}(q, t)$. The behaviour at small and large q is the same as in Eqs. (7.19) and (7.20). The authors give additional calculations and discussions on the physical quantities measured in our work of Ref. [26] (see Sect. 6).

7.3 Initial Conditions for the Disengagement: Contraction and Tube Diameter

As mentioned above and by several authors [37, 40], the q range of our experiment largely occupies the domain $q > 1/D$, D being the tube size, estimated for polystyrene to be the radius of gyration of a chain of molecular weight $M_e = 2 \cdot 10^4$, $D = 0.275\sqrt{M_e} = 40$ Å. The choice is then to:

(i) discard the data and wait for available larger chains and smaller values of q.

(ii) use some laws independent of qD, as reviewed in Sect. 6.

(iii) include the tube size in the calculated form factor. We first used the crude assumption of a cut-off: above the tube size, the chain is affinely deformed; below, it is isotropic. The cut-off was actually based on the chemical length, so that:

$$i - j < N_e \qquad \langle (r_i - r_j)^2\rangle = (i - j)\ b^2 \tag{7.24}$$

$$i - j > N_e \qquad \langle (r_i - r_j)^2\rangle = (i - j)\ \lambda_q^2 b^2 . \tag{7.25}$$

This gives a sharp departure from the original disengagement calculation. A smoother form can be obtained with the same threshold value for the chemical length, by replacing Eq. (7.24) by a crossover expression of the "end to end pulled chain" type (see below):

$$i - j > N_e \qquad \langle (r_i - r_j)^2\rangle = ((\lambda^2 - 1)\ ((i - j)/N)^2 + ((i - j)/N))\ Nb^2 \tag{7.26}$$

Figures are given in Ref. [39]. These calculations were compared with other data [9, 10].

However, we were later led to more precise calculations of the tube effect, especially as the description of the chain after the first process is exactly the one of a chain in a rubber using the classical models of the rubber elasticity theory.

7.4 Form Factor for a Deformed Rubber

Phenomenological Expression

The first attempt to calculate a deformed form factor was [41] to combine an end-to-end pulling with an affine deformation within the entire range in order to obtain the probability of finding the monomers i and j at the distance $\underline{r}_{ij} = \underline{r}_i - \underline{r}_j$.

$$p(\underline{r}_{ij}) = \exp\left[((x_{ij} - X)^2/\tilde{\lambda}_x^2 - (y_{ij} - Y)^2/\tilde{\lambda}_y^2 - (z_{ij} - Z)^2/\tilde{\lambda}_z^2)/|i - j|\, b^2)\right]. \tag{7.27}$$

Because only (i — j) is involved in this exponential term, the sum over i and j reduces to a sum over n = i — j only which leads to an expression of the same kind as the one for the isotropic form factor. The two limit behaviours are: the affine deformation corresponding to $X = Y = Z = 0$, and the end-to-end pulled chain $X \neq 0, \tilde{\lambda}_{x,y,z} = 1$ already treated by Kuhn and Katchalsky [42]. In plotting $1/S(q)$ versus q^2, the asymptotic expression ($qR_g \gg 1$) yields for the first case a change in the slope of the straight line, and for the second a vertical shift, as:

$$S(q) \sim 1/(q^2 R_{g\,iso}^2 + X^2/b^2 + 1)\,. \tag{7.28}$$

The general case is predicted to lie in between; some examples on the possibility of obtaining the different cases are given later, together with parallel orientation averages $\langle\cos\theta\rangle$ and $\langle\cos^2\theta\rangle$ (see Sect. 15).

Classical Models

In fact, this derivation [41] contains two main weaknesses. The first is the assumption that all chains between two crosslinks have the same end-to-end vector for the direction (parallel to the stretching axis) and modulus. This could be the case for a one-dimensional material, but in an entangled or crosslinked melt the end-to-end vectors are expected to have all directions. Moreover, a distribution of the moduli is also also sensible. For the isotropic case, the end-to-end vector distribution is Gaussian, and integrating the total distribution leads back to the usual average $\langle r_{ij}^2\rangle = |i - j|\, b^2/3$. The simplest assumption for a deformed material is an affine deformation of this end-to-end distribution:

$$P(R) = \exp -(3/2Nb^2(X^2/\lambda_x^2 + Y^2/\lambda_y^2 + Z^2/\lambda_z^2))\,. \tag{7.29}$$

Convolution of Eq. (7.27) (with $\tilde{\lambda}_{x,y,z} = 1$) by Eq. (7.29) leads to the conformation of a mesh inside a deformed network for the **junction affine model** often called Kuhn model [43], as shown by Ullmann [44] for the uniaxial extension, who gives:

$$p(x_{ij}) = \sqrt{(a_x/\pi)}\exp(-a_x x_{ij}^2),$$

$$a_x = 3/(2Nb^2|i-j|/N(1+|i-j|/N(\lambda_x^2-1))) \tag{7.30}$$

and similar expressions for y and z. Here, the distributions are also Gaussian, which allows to use the Gaussian approximation of Eq. (7.1) to derive the form factor. Following the same scheme, Pearson [45] elegantly remarked the possibility to adapt it with a few modifications to the *phantom network model* often called James & Guth model [46], as the distribution P(R) is still Gaussian with a different second moment.

Labeled Path

The second restriction [41,45] is that chains are attached to the network only by their two ends. In the case of a chain in a melt of mass $M \gg M_e$, it would be more realistic to apply the constraints by M/M_e points on the chain. A simple possibility is to divide the sum Σ over $n = |i-j|$ in two parts, one for $n < n_c$ and one for $n > n_c$, and use Eq. (7.24) for the first and Eq. (7.26) for the second. This was stated in Ref. [24], where calculations and curves are given for the parallel direction while for the perpendicular Eq. (7.25) was used instead of Eq. (7.26), used later [9]. Numerical evaluations are plotted in Refs. [9,10,29]. This calculation introduces a cut-off in the linear abcissa *along the chain*, which we called sliding blob, as no point is particularly affected along the chain.

The classical rubber elasticity model considers, however, that the crosslink points are particular, such that the cut-off occurs by these points in real space. The corresponding calculations for a chain obliged to pass by several crosslinks are recalled in Ref. [29]. The calculation for the junction affine model was accomplished by Ullmann for R_g and by Bastide for the entire form factor; for the case of the phantom network model, this was achieved by Edwards and Warner [47] using the replica method. Defining the number of crosslinks as two actually leads back to the expressions for only one labeled mesh; numerical evaluations are given in Ref. [29].

8 Comparison of Data with Calculations for Rouse and Reptation Models [9,10]

We will first discuss the data of set I. The comparison partially recovers the former comparisons carried out for the radius of gyration and intermediate regime. This comparison might be more quantitative while at the same time it requires, at one stage, knowledge of the characteristic times from other data.

The comparison with the *Rouse model* thus requires an estimation of the maximum time. That should be, in principle, the Rouse time $T_{Rouse} \sim M^2$. In fact, the calculated curve is compared and, if the fit is possible, one extracts from that a maximum time. The data of set I have been compared [9] as shown in Fig. 11. This yields:

— a first consistent possibility of comparison for short times ($t^{117} = 10$ s, 60 s). In

practice, the data are not sufficiently relaxed at high q. In the parallel direction, the data are too relaxed at small q, or not sufficiently at high q. The comparison, thus unperfect, leads to an estimate of T_{max}^{117} between 10^4 and $5 \cdot 10^5$ s. The estimated value $R_{Rouse} \propto M^2$ (see Sect. 4) gives T_{max}^{117} between $5 \cdot 10^3$ s and $5 \cdot 10^4$ s. The experimental value T_{max} appears slightly overestimated.

— an inconsistency for long t. Data for $t^{117} \sim 10^4$ s could overlap with theoretical curves for $t/T_{max} = 10^{-3}$ giving $T_{max} = 10^7$ s; and for $t^{117} = 10^5$ s, with curves for $t/T_{max} = 2 \cdot 10^{-2}$ giving $T_{max} = 5 \cdot 10^6$. These values of T_{max} are much larger than the estimations for T_{Rouse}, and even for T_{ter}. Moreover, using the same maximum time the disagreement is total in the perpendicular direction.

In summary, it is possible to fit the short time data with a constant reasonable value of T_{max}, but it is not possible to take into account the complete set I with the same value of T_{max}. Beyond the short time region, T_{max} always increases as t increases: i.e. the Rouse model is too fast for the data. Moreover, it is not possible to account both for the parallel and perpendicular directions (this corresponds to the observation in Sect. 6 that a $qt^{1/4}$ superposition is obtained for long t only in the parallel direction, while it is obtained for both directions at small t).

A comparison with the reptation model was performed [9,10] in two steps. A first dogmatic comparison assumed that $qD \ll 1$, which yields complete disagreement with the data. This led to the idea that the form factor might be much closer to the Rouse type. But accounting for the real value of qD ($qD > 1$ on a part of the q range), there remains only one fundamental disagreement, distributed over the entire q domain: the lack of observable contraction. We will finally see that suppressing the contraction effect — although it is completetly predicted by the model — allows the calculations to agree with the data better than using the Rouse model.

The dogmatic comparison is shown in Fig. 12. The form factor still reflects Eq. (6.9) at large q. The anisotropy of the function does no longer depend on q: this gives a plateau which decreases only with t, in sharp contrast with the data. A second discrepancy is visible at $q < 2 \cdot 10^{-2}$ Å^{-1}: the data lie clearly below the calculated curves.

The first discrepancy at large q can be suppressed within the framework of the reptation model, but with a realistic value of the tube diameter corresponding to Eq. (7.24). The result will be the disappearance of the plateau in the calculated curve $q^2S(q)$. A finite value of D is in fact the result of a Rouse motion during the period $(0, T_e)$, where $T_e \propto M_e^2$ is the Rouse time of a chain of mass M_e. Thus it resembles the Rouse model at this short T_e. At longer t the resemblance remains but the time decay is now slower and independent of q at large q, which is different from the Rouse model.

However, the second discrepancy still remains: the calculated curves still considerably exceed the data in *both* directions. That is, the contraction *should* be observable within the entire q range, while it is not. This confirms the result for the radius of gyration discussed in Sect. 5 (also see Sect. 13). It has been proposed [10,39] to take a contraction factor c equal to one. Thus, the third process starts from the situation already obtained at $t \sim T_e$. The initial form factor should be the one calculated through the Rouse model, at $t = T_e$; this is suitable when taking into account the tube size in Eq. (7.24) for $\mu(t) = 1$ with $N_e = M_e/m$ (i.e. $D \propto \sqrt{M_e}$). The experimental form factor at $t \sim T_e$ agrees in a first approximation with both calculations (q). For t longer ($\mu(t) < 1$), Eq. (7.24) shows reasonable agreement with data for large experimental values of t using constant values of N_e (200, i.e. $M_e \sim 20000$) and of T_{ter}

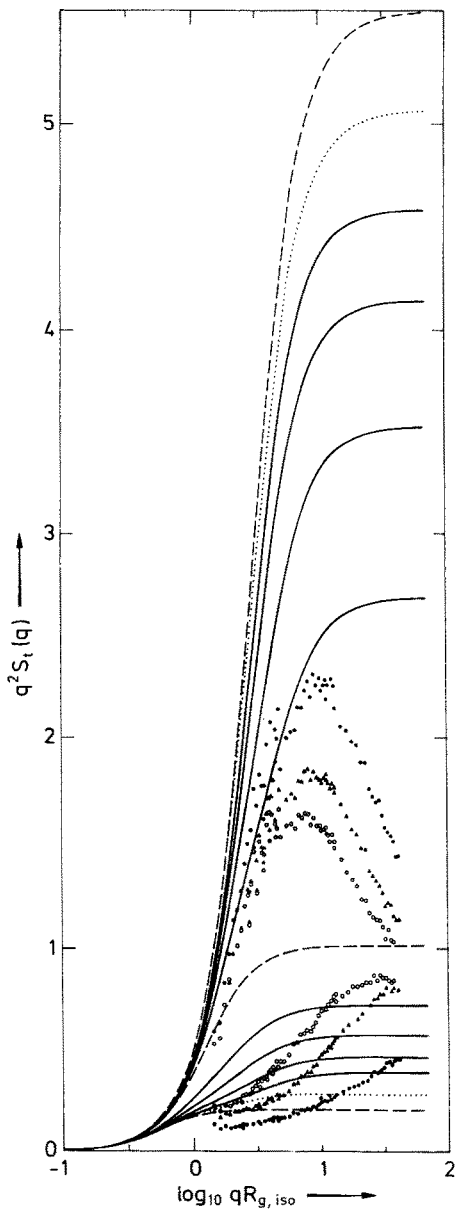

Fig. 12. Calculated form factor by assuming a disengagement of a contracted chain in a tube of zero diameter for $t/T_{ter} = 0$ (dashed line below and above), 0.1, 0.2, 0.4, and 0.8 (solid lines), and infinite (dashed line in the middle); data as in Fig. 3

($5 \cdot 10^5$ s) for the different t's (Fig. 13). This corresponds to the behaviour expressed in Eq. (6.8), also shown in Fig. 10. However, in the parallel as in the perpendicular direction the data seem more relaxed at intermediate q than the calculations: it is seen that not only the contraction did not occur, but that another process of relaxation took place instead. A similar effect is discussed in the following section, which may serve as a generalization.

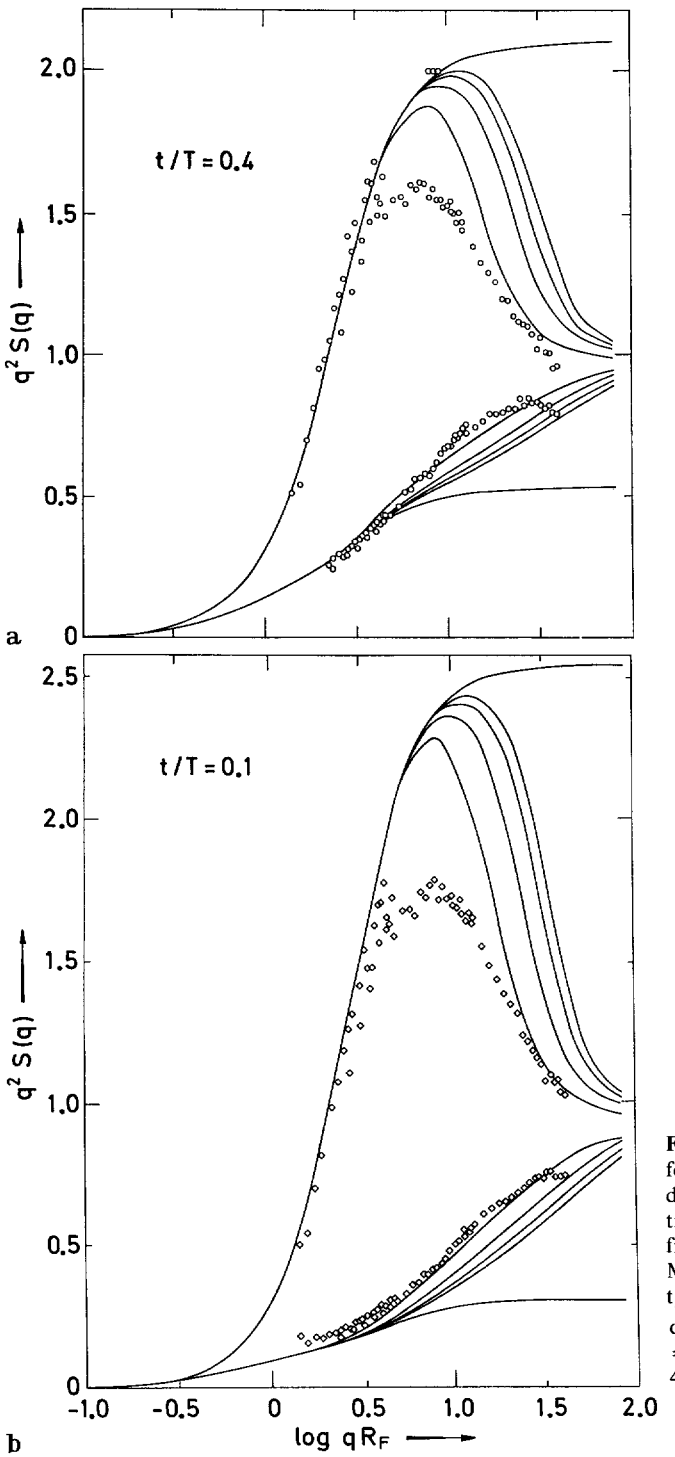

Fig. 13a and b. Calculated form factor by assuming the disengagement of a noncontracted chain in a diameter of finite value corresponding to M_e/M = 30, 60, 90, 120. **a** t/T_{ter} = 0.4, compared with data from sample 50; **b** t/T_{ter} = 0.2, compared with sample 46

9 Comparison of Data with Calculations Based on Classical Rubber Models

It is possible to investigate the initial state for the disengagement, or terminal process, in the form factor by exploring only a range of time t obeying both conditions:

$$t \gg T_e , \qquad t \ll T_{dis} . \tag{9.1}$$

For linear deformation, rheologists call this the plateau regime, because no important relaxation can be recorded. However, at large deformations, the rheological behaviour in a certain range is modified by an additional relaxation of an overstress, as observed by Osaki and others. This additional relaxation has been attributed to the contraction.

These conditions can be fulfilled by using high-molecular-weight specimens [29]: the labeled chain has a molecular weight of $2.6 \cdot 10^6$ dissolved in a $1.3 \cdot 10^6$ matrix (i.e. data set V). *If again we ignore contraction* (as we do not see it), we can compare the form factor in the regime of Eq. (9.1) to the one of a deformed rubber: this is indeed predicted by the Doi-Edwards theory at the end of the first and before the second process. The calculated curves were derived from the two classical models of Sect. 7,

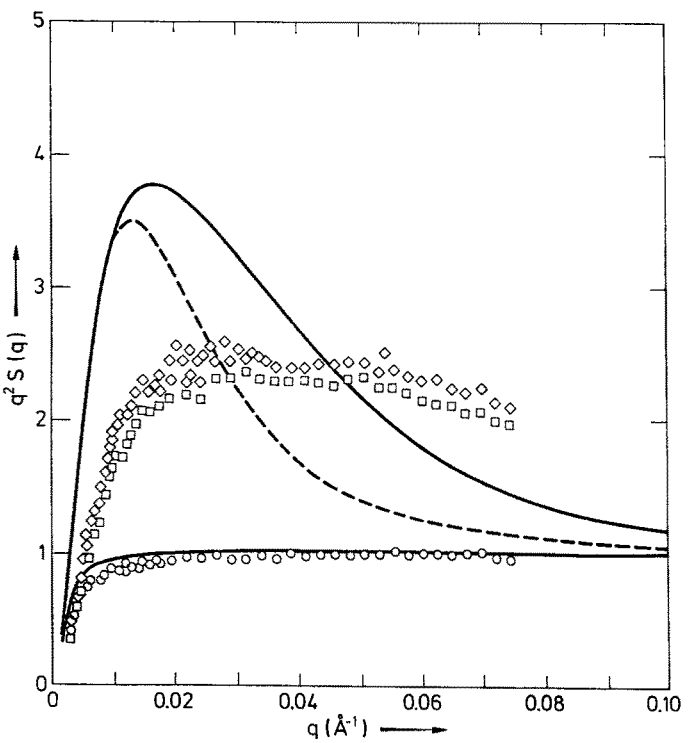

Fig. 14. Comparison of data for long chains in the plateau regime with the calculated form factor for a labeled chain ($M_{wD} = 2.6\ 10^6$) crosslinked in a rubber of mesh $M_e = 20000$. Solid line below, isotropic; above, junction affine model; dashed line, phantom network. Data: set VI (Table 1): ◇, $t^{140} = 10$ mn; □, $t^{140} = 40$ mn; ○, isotropic

the junction affine [43] and the phantom network model [46] instead of the crude cut-off of Eqs. (6.23), (6.24). The molecular weight of the mesh was taken as $M_e = 2 \cdot 10^4$; the stretching ratio was $\lambda_{//} = 4.6$, leading to $\lambda_{per} = 1/\sqrt{4.6} = .46$. Two disagreements appear (Fig. 14): one at large q (data exceed the values on the curve), and one at small q, in which we are mainly interested:

— the data at small q are clearly below the calculated curves: even at $q \sim 5 \cdot 10^{-3}$ $Å^{-1}$ the chain is less deformed than predicted by the phantom network (dotted line), which already predicts a lower deformation than the junction affine model (solid line); the Flory-Erman [48] model which is intermediate, would then also disagree. It is as if the loss of affineness does not start at q of the order of the inverse of the mesh size, but that it spreads on a wider q range down to values smaller than the ones observed. The lack of deformation can be seen as an additional relaxation, not predicted by the models; no hope of improved agreement can be expected from introducing the contraction process in the calculation; this would enhance the discrepancy at least as far as the perpendicular direction is concerned.

— the data at large q are more deformed than the calculated values as if less freedom than predicted is actually available.

It is possible for this experimentally observed hyperrelaxation to correspond to a process occurring in a time $t \sim T_{Rouse}$. It could then produce the decay of the overstress, observed by Osaki, by other means than by retraction. In that case, the Doi-Edwards model would have to be modified (see last part of Sect. 13). We will now see that excess deformation also occurs for deformed crosslinked materials, and melts and rubbers can appear to behave similarly under certain conditions.

10 Direct Comparison of Melt and Rubber

10.1 Deswollen Gels and Stretched Melts

The classical rubber models have also been used to compare data from a deformed *crosslinked* polystyrene [29]. This was done starting from a gel, crosslinked by gamma rays from a solution containing 10 % large PS chains of $M_{wD} = 2.6 \cdot 10^6$ of which 1 % were deuterated, in a radioreactive solvent. In the swollen state the chain appeared Gaussian (the solvent being a theta-solvent); after deswelling by drying the sample experienced a compression of $1/\sqrt[3]{10} = .46$ (close to the extension ratio of the melt of set VI). The deuterated chains provide the form factor of a long path in the network. The molecular weight of the mesh is carefully extrapolated from a complete set of diffusion coefficients and swelling ratios for calibrated gels; M is found to be close to 35000. Again, as for melts in the rubber plateau, the calculated curve, now for $M = 35000$, shows an important discrepancy with the data. The data appear also less deformed at low q, and more deformed at large q. The conclusion of Ref. [29] is that the two behaviours, for melts and for rubbers, appear to be physically similar. This last point led to another closer comparison between crosslinked and uncrosslinked melts, briefly outlined in the following.

10.2 Stretched Melt and Stretched Rubber

For a direct comparison one must have samples of the melt and dry rubber containing the same labeled chains. This was achieved by preparing samples of melt containing 10% of $M = 2.6 \cdot 10^6$ deutered chains in 90% of $M = 1.3 \cdot 10^6$ non-deuterated chains. Half of the samples were then slightly swollen ($Q = 1.2$), gamma-crosslinked, and then washed and dried. Half of the samples were not irradiated and let in the uncrosslinked state, and half was prepared in the crosslinked state, all of them in the same final shape. They were subsequently deformed under the same conditions of stepstrain at $T > T_g$, and relaxed for equal times before being quenched. In the preliminary experiments [49,49bis,60], three values of time and three values of λ (1.46, 2.14, 4.6) were used; representative results are given for $\lambda = 2.14$ in Fig. 15. It is seen that the evolution of the form factor is very similar in the two cases. For very short t (1 mn at 116 °C) there is a difference at large q which can be related to a difference in T_g, suggested also by the stress behaviour. At higher temperatures (1 mn at 150 °C) the form factors overlap. For the rubber, the longest t (30 mn at 150 °C) — which has only recently been experimentally attained for the melt — leads to a form factor again less oriented than the prediction by the phantom network model.

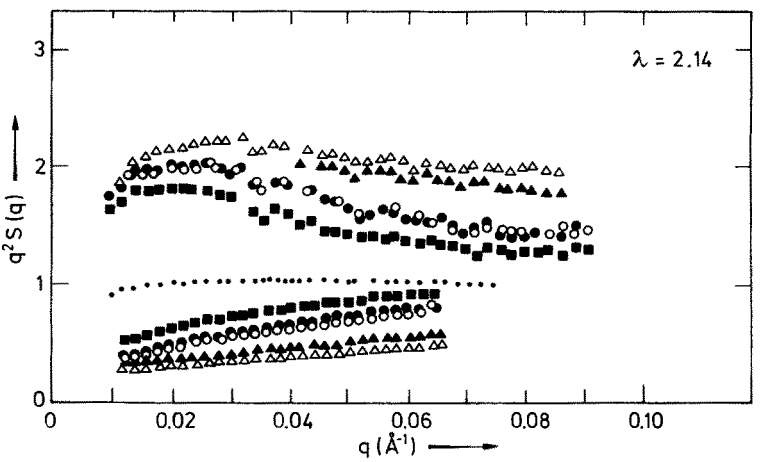

Fig. 15. Form factor from the same labeled path ($M_w = 2600000$) in melt (hollow symbols) and crosslinked melt (full symbols); $t^{16} = 30$ s (△), $t^{115} = 1$ mn (○) and 30 mn (□)

The same features are observed for $\lambda = 1.46$ and 4.6; however, while rubber and melt still precisely overlapp, the discrepancy with models is enhanced by increasing λ. A detailed comparison with models [49bis,60] shows that

— it is possible to fit grossly data in the perpendicular direction with a junction affine model and a crosslinking rate somewhat larger than the one expected from other characterizations (swelling ratio).

— the same sample in the parallel direction will scatter much more following the phantom network model, and with a crosslinking rate now 5 times weaker, thus noticeably smaller than extracted from the swelling.

11 Effect of the Molecular Weight. Alternative Tests of Reptation

In this section we directly compare the data for different molecular weights without using any predicted law or any calculation; this is an alternative for testing some intrinsic concepts of the current theories.

11.1 Comparison Between Mixtures of Different Molecular Weight, Keeping the One of the Host Chains Equal to the One of the Labeled Chain

Available data allows us to compare between shorter chains (M_{wD} = 95000) in a similar matrix (M_{wH} = 105000) and between larger chains (M_{wD} = 780000) in a similar matrix (M_{wH} = 760000) for all times. For short times, we have a satisfactory overlapping within the uncertainty of the two form factors for several equal values of t, at large q. This is in agreement with all models: at short times the conformation changes only for small sizes along the chain, independent of the size of the chain. For longer times, the form factors for the different molecular weights separate within the entire range of q: even the evolution at large q is slowed down at the longest time of the macromolecule. This is consistent with the tube model, but does not coincide with the Rouse model, for which the rate of decay depends only on q, whatever the size of the chain. The time at which the separation begins is of the order of 100 s at 117 °C. This needs to be compared to T_e^{117}, estimated as 10–50 s. Again we find, without any delicate model comparison, an agreement with the idea that the free chain behaviour ceases at T_e.

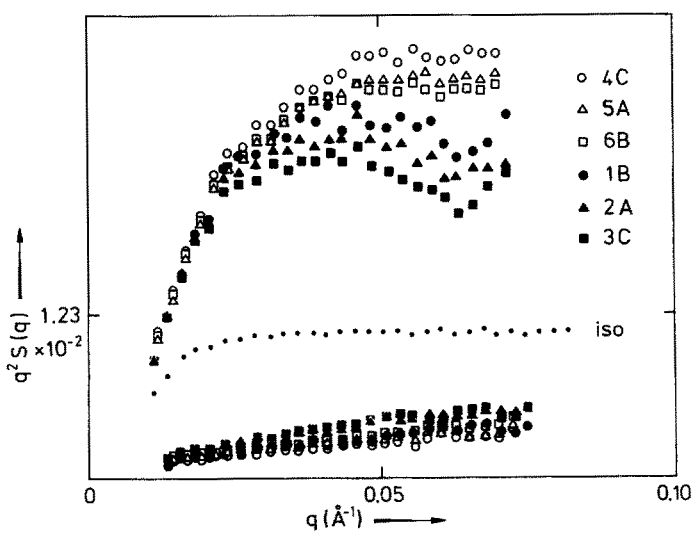

Fig. 16. Form factor from the same labeled path (M_w = 400000) in matrices of different molecular weights: ○, 1600000; △, 400000; □, 200000. Hollow symbols are for time 1 mn at 122 °C, full symbols for 1 mn at 126 °C

11.2 Effect of the Matrix: Variation of the Molecular Weight of the Host Chains without Changing the One of the Labeled Chain

A first insight into this effect is allowed by the data of set II and III, obtained at the same time, under same conditions of stretching and scattering. The labeled chain was $M_{wD} = 95000$ and the matrices $M_{wH} = 105000$ and 1300000, ten times more (one thousand more for the terminal times). Comparison indicates a very good coincidence over the entire time range explored up to about $T_{ter}/50$ (T_{ter} being the terminal time $M_{wH} = 105000$). Only the longer times produce a considerable difference; for this case the matrix of the sample being essentially constituted of small mass material may have slightly changed of shape during the long relaxation period.

Experiments were carried out with four blends: $100000_D/100000_H$, $100000_D/600000_H$, $60000_D/600000_H$, and $600000_D/100000_H$. A matrix effect was noticed for both deuterated chains [30]. A more complete experiment investigated the matrix effect at longer times [31]. The same labeled chains, of medium molecular weight $4 \cdot 10^5$ ($M/M_e = 20$), were dissolved in four different matrices: $M_{wH} = 2 \cdot 10^5$, $4 \cdot 10^5$, $6 \cdot 10^5$, and $1.6 \cdot 10^6$ (see Table 1), with narrow polydispersities (1.15). The samples were then stretched under the same conditions, and relaxed for equal times. For T = 122 °C and $t_R = 1$ mn, the form factors are located close to each other in Fig. 16 (the largest molecular weight being a little less relaxed). For T = 128 °C and $t_R = 1$ mn, a systematic effect of the matrix is seen: the chain appears more relaxed for smaller molecular weights of the matrix. This also appears in the values of the radius of gyration (detailed data to be published). Here, only two general remarks:

— in such an experiment great care must be taken of the polydispersity of the samples: wide distribution could lead to a non-neglectible amount of very small chains; these could be more for smaller average molecular weights and would lead to faster relaxation.

— the fluorescence measurements of Tassin et al. [16], who used PS chains with an anthracene probe grafted in the middle, dissolved in different PS matrices, show a matrix effect. We chose the same samples as matrices, a deutered chain of about the same length as their grafted one, and corresponding temperatures and times to allow a comparison between the two experiments. The tests appear consistent, at first sight; neutron data appear however more sensitive to a matrix effect even when M_{wH} is very large. We do not see such a simple saturation effect when increasing M_{wH} as claimed by Tassin. Direct quantitative comparison is difficult without involving a model, as will be briefly pointed out in Sect. 15.

12 The Observation of Anisotropy

Up to here we have mainly considered the data grouped in angular sectors, slightly narrow, centred on the direction of q parallel or perpendicular to the stretching axis, $\vec{s}$. We now want to focus on:

(i) the possible errors arising from this regroupment method

(ii) the potential information content of considering *all the data*, especially via isointensity maps.

12.1 Error from Angular Regrouping

When the cells are regrouped in an angular sector centred on 2 given φ — assuming an accurate control of sample alignment [9] — an uncertainty results from the width $\delta\varphi$ of the sector. The usual situation, at large deformation ratios, is the following: around the parallel direction, the isointensity curves slowly vary with φ; thus, the error when using large $\delta\varphi$ (20 deg.) is small. On the opposite, the φ dependence around the perpendicular direction is much more acute, and care must be taken. We usually find that $\delta\varphi = 5$ deg and $\delta\varphi = 10$ deg do not give any relevant difference. A computerised extended procedure of control was designed at ILL (P. Lindner): the value at each q can be plotted as a function of $\delta\varphi$ and extrapolate at zero value. Linear extrapolation appears to be possible, while this is not justified completely, and thus maybe confusing. On the other hand, it can be especially useful for poor counting as it is a way of using more cells of the detector. We will now describe other possibilities of using the detector.

12.2 Analysis of the Dependence on Angle φ: Isointensity Curves. The Strange Losanges. Extinction Angle

Instead of restricting ourselves to $\varphi = 0$ deg and 90 deg, corresponding to the perpendicular and parallel directions of q with respect to the stretching, one should explore all values of φ. A first procedure would be to make angular regroupments for a reasonable number of φ values (about ten for a width of 10 deg). This treatment, which is long, can be used for two purposes:

— If we know in advance the shape of the isointensity curves, testing and then fitting it on the whole detector will provide more accurate measurements. Two levels of exactness can be used. The most exact will impose a shape: one example is the ellipse with a ratio between the two axes of $\lambda/\sqrt{\lambda} = \lambda^{3/2}$; then we take an elliptic ring and group all cells inside this ring: the accuracy is then the same as for isotropic spectra when one regroup the cells inside a circularring! Earlier [23], we extracted a given value S for each value of q and for each φ, in the X, Y plane, by smoothing the data, drew each isointensity curve and fitted it to an ellipse in order to extrapolate more accurate values of S(q) in parallel and perpendicular directions. We later ran a program for an analytical fit to the ellipse (at ILL, Grenoble). Improving the accuracy is delicate and there might be a distorsion of data by these methods. One reason might be simply that assuming a priori an analytical shape is more than unusual.

The small t_R/T_{ter} data — inclusing data of earlier work — give elliptic shapes. They are characterized by their axis ratio, which can be compared to the affine value $\lambda^{3/2}$. In the q, t range where both the parallel and perpendicular S(q) are close to the affine value, the axis ratio has the affine value (even in the intermediate regime for the parallel or in the Guinier regime for the perpendicular). As soon as the affine variation is abandoned in one direction, the axis ratio decreases with time and with q, but curves remain elliptic [20, 23, 24] (also see Fig. 17a). A second set of data, obtained recently, involves large durations, for various situations, e.g.:

— For molecular weights equal for labeled and matrix chains, when durations are about one tenth of the terminal time (sample # 50 of set IV).

— For labeled chains in a matrix of larger chains, when times are attained which are

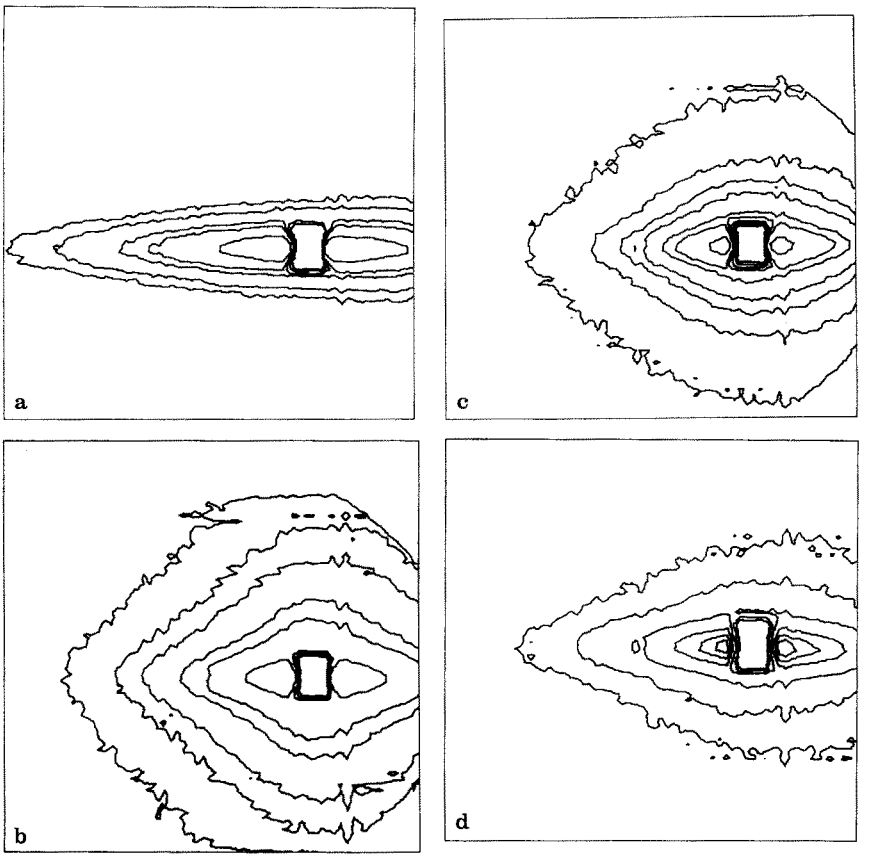

Fig. 17a–d. Isointensity lines on the two-dimensional detector. **a** $\lambda = 4.6$, T = 110 °C, t = 1 mn, crosslinked sample (uncrosslinked gives the same pattern); **b** same crosslinked sample, $\lambda = 4.6$, T = 150 °C, t = 30 mn; **c** same sample, same λ, T, t but in addition return to $\lambda = 3$, at T = 110 °C, which took t = 7 mn; **d** melt, $\lambda = 4$, $M_{wD} = 400000$ in $M_{wH} = 1600000$, T = 134 °C, t = 5 mn

comparable to the terminal time of the labeled species, while the sample still behaves like a solid.

— For a crosslinked polystyrene (see Sect. 10) when the sample is relaxed indefinitely, in principle.

Representative curves are displayed in Fig. 17b, c, d. One clearly sees a losangic shape, instead of an elliptic one. Our explanations for that experimental fact are yet insufficient. A losange appears as a combination of ellipses of different axis ratios. Some chains could be more relaxed than others. The sample could be inhomogeneous on a very small scale, as predicted by some theories [50]. Also for rather polydisperse samples, the smallest chains could have become quasi-isotropic, while the largest being still very anisotropic (this is possible even for not too high polydispersity because of the $M^{3.4}$ law for the terminal time); a naive explanation could involve reptation which during disengagement provides a mixture of deformed chain parts in the middle of the chain and of isotropic parts at its ends. For cross-linked systems these proposals have to be replaced by an effect of pendant chains. We have done recently calculation

for rubber deformation models including this effect: a lemon shape may be observed, never a losange shape, which we obtained only in a particular combination of orientation of end to end vectors R, only parallel or perpendicular to the elongation [49 bis].

"*Extinction*" *angle.* It is interesting to note that the assumption of affine displacement of the mean positions of the junctions lead always to a dependence on λ and θ of the type

$$\lambda^2 \cos^2 \varphi + 1/\lambda \sin \varphi$$

for both junction affine and phantom-network models. Then an extinction value $\varphi^*(\lambda)$ always exist for which the form factor should be $S(q, \varphi^*) = S_{iso}(q)$. Disengaged parts of chains, pendant chains, will give contributions, of isotropic smaller Gaussian chains. The resulting signal could always be analysed as the one of isotropic polydisperse distribution of chains, and in particular $q^2S(q)$ should be a plateau at large q. In our data for rubber, an agreement with that behaviour was found for $\lambda = 1.46$, but *not for 2.14 and 4.6.*

We propose finally another way of exploring the φ dependence, which is by analysing, during the neutron experiment, the ω dependence. Namely, we vary the angles of the axis of the incident neutron beam and the stretching axis: this is, e.g. a way to obtain access to the large values of the distances ($R_{g//}$) in the parallel direction.

13 Summary of the Test of Reptation

The reptation model in the melt predicts three regimes. Let us recall the predictions for $S_t(q)$ for each regime by estimating each time range for our experiment, and then — keeping in mind the large uncertainty of the estimates — search for any predicted behaviour in the corresponding range.

The first predicted regime is a Rouse relaxation, with the normal Rouse time distribution T_{Rouse}/p^2, where T_{Rouse} is the maximum Rouse time of the whole chain. At any time t, it has acted only upon sizes smaller than $r^*(t) \propto R_g\,(t/T_{Rouse})^{1/4}$. The relaxation must stop when $r^*(t) \sim D$, i.e. when t is equal to the maximum Rouse time of a chain of mass M_e, $T_e \propto M_e^2 \propto D^4$. At small distances it must give exactly the same conformation whatever the value of the mass M of the chain, given that $M > M_e \sim 2 \cdot 10^4$. Our estimate for T_e^{117} (i.e. T_e at 117 °C) is 10 s to 100 s. For the range from 5 s to 200 s, the data show a rapid relaxation at large q, and a quasi nil relaxation at small q: R_g varies a few percent for $M_D = 10^5$, and not at all for $M_D = 7 \cdot 10^5$, and the same q range shows no relaxation for $M_D = 2 \cdot 10^6$. This is only contradicted for $M_{wD} = 3 \cdot 10^4$, close to M_e. In the q range of fast relaxation, the data for the masses 10^5 and $7 \cdot 10^5$ overlap (not tested for $2 \cdot 10^6$ because of a different stretching ratio). The intermediate regime appears to comply with a superposition law (Eqs. (6.4), (7.11)) of a unique parameter ($qt^{1/4}$). The fit to a form factor calculated form the Rouse model is acceptable at large q using a Rouse time for the whole chain within the uncertainty range of the estimates. In the case $M_{wD} = 7 \cdot 10^5$, for $t^{117} > 500$ s, this fit is no longer possible without changing the value of the Rouse time and progressively removing it out of the uncertainty range. The relaxation at large q appears to become slower while the radius of gyration starts to decay; the $qt^{1/4}$ super-

position is not possible. For $M_{wD} = 1 \cdot 10^5$, the Rouse and reptation models give more similar behaviours, so do the data. In summary there is a good agreement with this first regime, inside and only inside a range of q, t, M corresponding to the theoretical expectation.

The second predicted regime is an equilibration inside the fixed tube. The chain feels only the finiteness of its own length, not the one of the tube. Thus, inside the contorted tube, this is a one-dimensional Rouse motion of maximum time $T_{Rouse}(M) \propto M^2$. The motion should follow $r(t) \propto t^{1/8}$. For a deformed sample the equilibration corresponds to a contraction inside the tube. As this latter is three-dimensionally contorted, it corresponds to an increasing by a factor $c(\lambda)$ of the density correlation function $\langle c(0)c(r)\rangle$ for any direction of r. In terms of scattering this will produce, in particular, a decreasing of the radius of gyration in any direction, and, more generally, the form factor of a labeled path through a deformed phantom network, but with a density increased by a factor $c(\lambda)$. This will be the case when the equilibration is completed, at the end of the process, i.e. when $\exp(-t/T_{Rouse})$ is neglectible ($t/T_{Rouse} > 5$).

For $M_{wD} = 7 \cdot 10^5$, $T^{117}_{Rouse}(M)$ is estimated to be $(5 \cdot 10^{-3}$–$5 \cdot 10^4$ s); for the range $t^{117} = 200$ s to 10^4 s, the data for both uniaxial extension and shear deformation do not agree with the theory. A slowing down is observed around the reduced time at 117 °C of $t^{117} = 200$ s, and then the motion $r(t) \propto t^{1/8}$ could agree with the experimental variation (see Fig. 10). However, S(q) relaxes by a continuous increase of $S(q_{//})$ and continuous decrease of $S(q_{per})$; it is very clear on measurements of $R_{g\,per}(t)$ and coincides with the behaviour within the entire q range; contraction is not observed.

Moreover, a relaxation in the opposite direction *is* observed. This one is sufficiently significant to establish the following situation: not only does the form factor not follow a contracted labeled path ($c > 1$) in a phantom network, but it does not either comply with the Gaussian density ($c = 1$); i.e. it is even more relaxed than predicted by the model of rubbery deformation with no contraction, assuming the less oriented, so-called phantom network. The argument that the third process could have already started is extremely weakened by more recent experiments: the same effect is also observed for larger M, $2 \cdot 10^6$, for which the ratio M/M_e is much larger, ~ 100, theoretically corresponding to a strong decoupling of the second and third process. Finally, the form factor of a labeled path of same molecular weight in a *crosslinked melt* was found to be very similar, though no terminal process should occur. Also, still in that regime, we have observed an effect of the matrix on the relaxation of a considerably long chain $M_{wD} = 4 \cdot 10^5$ among chains of larger M. This effect is not predicted by the Doi-Edwards model.

The third predicted regime is the disengagement of the chain from the initial deformed tube: here, the finiteness of the tube becomes relevant, and the maximum time is $T_{dis} \propto M^3$. In practice, it is expected to be equal to the terminal stress relaxation time, though this latter is actually proportional to $M^{3.4}$. The main feature in the case of deformed materials is the inhomogeneous structure of the chain which appears as a triblock copolymer isotropic-anisotropic-isotropic. Quantities related to sizes smaller than $\beta(t)$ of the blocks behave as in the case of adding isotropic and anisotropic parts. This is the case for the theoretical behaviour at $q > 1/\beta(t)$, which gives $S_t(q) - S_\infty(q) \propto F(q)\,\mu(t)$. The rate of growth of the isotropic part is $\beta_{iso}(t) \propto \sqrt{1 - \mu(t)} \propto t^{1/4}$ at small $t/T_{ter} \cdot \mu(t)$ is asymptotic to $\exp(t/T_{ter})$ at long times, and so is the variation of the reduced squared radius $(R_g(t)/R_{g\,iso})^2 - 1$.

Experimentally, the maximum achieved value for t is T_{ter} only for $M_{wD} = 3 \cdot 10^4$ chains, which is too short for the reptation test. For $M_{wD} = 10^5$ and $7 \cdot 10^5$, it is $T_{ter}/10$. The reduced squared radius variation appears close to an exponential in all cases, and the decay times are close to the estimated (and also measured for $M = 7 \cdot 10^5$) stress relaxation time. But this is not a key test of the reptation theory: for example, the Rouse model predicts also the same time variation of both quantities at long times (within a factor two for the terminal time).

A more exclusive test is the behaviour at large q. As both large enough t/T_{ter} and M/M_e are needed, only data for $7 \cdot 10^5$ can be used, and they agree with the factorisation law of Eq. (6.8) within the uncertainty of the measurement. This observation is strengthened by the fact that one obtains a terminal time equal to both the one of relaxation of the reduced squared radius and the one of relaxation of the stress. In summary, at that level, the few existing data agree with a disengagement process starting from the situation observed at $t \sim 10^4$ s, this latter disagreeing with the second process. This is also observed by comparing to calculated form factors for the disengagement.

A puzzling $qt^{1/4}$ superposition for this range of time has been reported. A possible explanation [9] may be that the threshold q value for the validity of Eq. (6.6) is $q^*(t) = 1/\beta(t) \propto t^{1/4}$ at short t. This was then observed only in the parallel direction because in the perpendicular, q^* is very close to $1/R_{g\,per}$. The curves calculated for $D = 0$ do not lead to a real superposition, which would only result from a finite tube size. In that matter, other experiments are needed at longer times; technically this would imply to remove the limitation of the chemical degradation which becomes as fast as the mechanical relaxation (see Sect. 2).

In summary, the experimental data contain two regimes which can coincide, both for their time range, and for the time dependence of $S_t(q)$ inside that range, with the first and third process of the tube model, respectively. In both cases, almost for the third regime of disengagement, the experimental range should, however, be extended for a better check.

A different regime, between the two former ones, should correspond to the second process of the tube model, with respect to the time range. This regime is widely explored in our experiment. But for this regime the data for $S_t(q)$ do not agree with the theory for the time dependence. This stands in contrast to the very good agreement with the tube model observed for rheological data [51, 52]. It is still necessary to find ways of combining the two experimental behaviours. We propose the following: At the end of Sects. 9 and 10 it was shown that deformed rubber (by deswelling a solution after crosslinking or stretching a dry rubber) exhibits a deformation inside the q range, lower than predicted by both the two classical models, i.e. the Kuhn model with affinely displaced junctions [43], and the model of James & Guth and Deam & Edwards [46] where only the mean positions of the junctions are displaced affinely. Moreover, the form factor of the same labeled path in a melt showed a behaviour close to the one of the rubber. This prompts us to propose that:

— The idea of similarity between a melt in the plateau regime and a rubber can be maintained.

— For both materials, the classical models for rubber elasticity predict a too high deformation on the observed scale. This is because additional rearrangement of the chains occurs on a larger scale than that of the size of the mesh.

— This additional rearrangement, when occurring in the melt, will produce a "tube rearrangement" in the time range of the second process. This would allow the linear density of the chain to equilibrate with no (or much less) retraction, and still the decrease in stress would be identical, the initial and the final value being the same.

The M^2 dependence found by Osaki et al. could have two explanations:

— Either the tube rearrangement leaves a low linear density to relax at the equilibration time $T_{Rouse} \propto (M/M_e)^2$;

— Or the rearrangement is also a Rouse process of longer times $T_{ter\,rearr}(M) \propto (M/M^*)^2$.

14 Local Effects

In the previous sections we always supposed $q \ll 1/b$, where b is the persistence length. For $q > 1/b$, all universal laws for polymers, such as scaling laws [53], are no longer valid. This is the same for our concern with the calculated form factors (Sect. 7); the asymptotic law (Sect. 6) for the Rouse (disengagement) model can be maintained if $\varrho > b$ ($D > b$). Recent progress is SANS underlined the limitation of universal laws, by improving not the spatial resolution ($1/q$) but the *chemical resolution*. Instead of using completely labeled polystyrene (monomer $-C_8D_8-$, called PSD8), Rawiso used polymers with only some of the hydrogen nuclei replaced by deuterium nuclei:

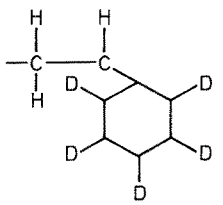

(PSD5)

and

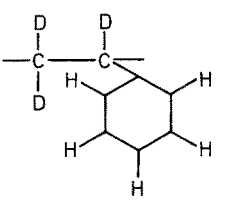

(PSD3)

First experiments were performed on dilute solutions in good solvent: here, in the so-called intermediate regime (see above), the measurement of S(q) using PSD8 chains gave a plateau $q^{1/\nu}S(q)$ versus q, with $\nu_{exp} = 0.6$ [54]. This was predicted by the scaling law $S(q) = 1/q^{\delta}$, where δ, the fractal dimension, is here equal to $1/\nu$. Using PSD3 ("labeled backbone"), a surprising effect arises: the plateau $q^{1/0.6}S(q)$ completely disappears, hardly signed by an inflexion point after which the curve continues to increase. Using PSD5, on the contrary the plateau is replaced by a maximum after which the curve decreases. These two facts led to the idea that the plateau results from a fortunate compensation between two effects:

— The persistence length effect, which will increase $q^{1/\nu}S(q)$ as q increases, tending to a rod behaviour ($S(q) \propto 1/q$). A crude reasoning would predict the onset of this behaviour at $q \cong 1/b$, b being the persistence length. More exact calculations using a worm-like chain show that this effect would be visible by SANS at rather low q (0.3/b, i.e. $3 \cdot 10^{-2}$ Å^{-1} for PS, where b = 12 Å).

— The axial radius effect, due to the thickness of the chain. The form factor is then

multiplied by the Patterson function of the density distribution perpendicular to the axis:

$$S(q) = S_0(q)\, F(q) \tag{14.1}$$

where F(q) is a decreasing function of q. It can be expanded as:

$$F(q) = 1 - q^2 R_c^2/2 + 0(q^4 R_c^{'4}) \quad \text{for} \quad qR_c < 1\,, \tag{14.2}$$

where R_c is the axial radius.

The D8, D5, and D3 curves result from different values of $R_{c\,app}$, the apparent radius due to the contrast between labeled and unlabeled nuclei (a complete description is given in Ref. [55]); one must note that the D3 chain does not strictly correspond to the naked backbone because of the difference between the benzyl ring and the solvent at the level of their "density of diffusion length" (the equivalent for neutron of the indice for light); it will be obtained by "contrast variation" using mixtures of H solvent and D solvent).

A similar effect occurs in the case of a melt ($\delta = 1/\nu = 2$), as observed for small chains. Onleading investigations employed larger D8, D5, and D3 chains ($M > 10^6$) dissolved in a deuterated matrix (this reduces the incoherent scattering by a factor of 40, the substraction of which is very delicate at high qs). Isotropic and deformed ($\lambda = 3$) melts have been observed. Representative data for D3 chains are given in Fig. 18. The $q^2S(q)$ plateau is not obtained for isotropic melts containing D3 or D5 chains (in fact, even for any D8 data the plots show a decrease at $q > 10^{-1}$ Å^{-1}). For deformed polymers the pattern is also unusual, as the parallel and perpendicular form factors tend, as for D8, to return to the isotropic form factor at large q. This clearly shows that local effects at large q are not negligible.

According to Eqs. (13.1), (13.2), the ratio of the form factors for the two different species PSD_i and PSD_j will be:

$$\frac{S_{D_i}(q)}{S_{D_j}(q)} = \frac{F_{D_i}(q)}{F_{D_j}(q)} \sim 1 - q^2\, \frac{(R_{ci}^2 - R_{cj}^2)}{2} + 0(q^4 R_c^4) \tag{14.3}$$

The q dependence of the ratio is determined by using a Zimm plot or a Guinier plot as for the usual measurement of the radius of gyration (though the values of q are much larger here), and $R_{ci}^2 - R_{cj}^2$ is calculated.

This works for our preliminary results, as well on the $S_{Di}(q)$ than on the 3 quantities, which can be extracted from S_{D8}, S_{D5} and S_{D3}, quoted $S_{BB}(q)$, $S_{B\varphi}(q)$ and $S_{\varphi\varphi}(q)$ corresponding to the correlations backbone-backbone, backbone phenyl and phenyl-phenyl. An interesting result for example, is that $\frac{S_{BB}}{S_{\varphi\varphi}}$ — or, more directly $S_{D8}(q)/S_{D3}(q)$ for example — is a different function of q for the isotropic melt, the deformed melt in the perpendicular direction (faster decreasing) and in the parallel direction (even faster). This means that the correlations would be modified at the local scale [61].

In the isotropic case it is possible to extract the R_{C_i}'s from a fit to (14.1) where $S_0(q)$ will be the form factor of a wormlike chain. Because correlations appear modified

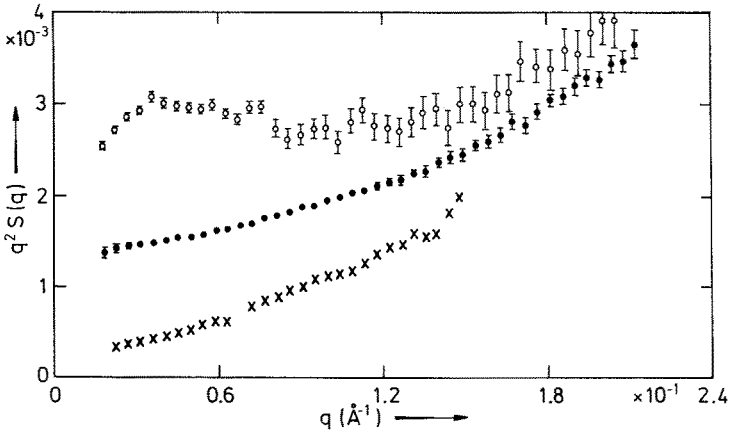

Fig. 18. Form factor of a PS chain (M_w = 1000000) labeled only on the 3 carbons close to the backbone, in isotropic (○) and stretched sample (per ○ para ×)

it is not possible to use these values of R_{c_i}'s for the deformed case: it follows that $S_0^{(deformed)}$ cannot be extracted that way. One would need a calculation of a deformed wormlike chain for further progress.

Here, the data of Fig. 18 can be used to evaluate the beginning of the local range in q: the effect is around 1 % at $q = 3 \cdot 10^{-2}$ Å^{-1} and 5 % at $q = 7 \cdot 10^{-2}$ Å^{-1}. This latter limit will be assumed at the upper boundary of the subentangled regime. Its influence on the former conclusions is:

— In the case of the Rouse model another concept is involved, the "Rouse subchain" which is the elementary unit. It is not clear how large this is, compared to the persistence length; we assume it to be of the same order[1].

— In the case of the disengagement model, Eq. (6.8) holds *a priori* even at large q, thus also in the local regime, no matter whether $S_{shortt}(q)$ and $S_{iso}(q)$ are affected by the local effects.

— of course, effects such as a local nematic field (see Sect. 15) would be sensitive at these q and modify $S_{shortt}(q)$, but that implies a physical modification of the model.

15 Comparison with Other Techniques

15.1 Difficulties in Investigating the Melt

In the Introduction it was mentioned that most other techniques are unsuitable to study melts in the range T_e, T_{ter}. Welding studies ($t \sim T_{ter}$) and self-diffusion experiments ($t \gg T_{ter}$) were reviewed by de Gennes [26] together with results from other techniques for solutions and also for long times. Neutron Spin Echo suffers from an

* The same problem is encountered for inelastic neutron scattering. A Rouse behaviour ($\tau(q) \propto q^4$) is surprisingly observed for a q range larger than 10^{-1} Å^{-1}, sensitive to both the Rouse subchain and the persistence length.

available range of too short times, and also too large q. Only recently, a tube effect has been described (J. Higgins et al.) resulting from the very small tube diameter of PTHF, but this remains in the range of $t \sim T_e$. Apart from viscoelastic measurements, which still hold a great potential for research, another set of techniques may allow comparison to the neutron data in same time range: this technique employs no probe (birefringence) or does use probes in the absence of demixtion: very weak concentrations (10^{-6} for fluorescence polarisation [17]) or nuclear labeling (deuteration; infrared dichroism [17] and deuterium magnetic resonance [56]). These methods all measure the *orientation* of the chain on a *small scale*. It seems useful to add some comments on the relation which can be established between these methods and neutron scattering; especially considering the relation between $\langle\cos^2\theta\rangle$ and S(q):

The optical methods measure the second moment $\langle\cos^2\theta\rangle$ of the orientation distribution function f(cos θ) of the monomers or of a probe. A first difficulty is to relate this function to the orientation function of the statistical unit: one might need to use a model of the chemical arrangement of the chain, or to establish a proportionality coefficient in the case of a probe. Then there can not be, at our knowledge, any direct relation (i.e. not model-dependent) between $\langle\cos^2\theta\rangle$ and S(q). This can be illustrated by three examples, corresponding to different models of chain conformation.

The first example is the totally affine deformation of the isotropic Gaussian conformation. In that case the deformation is the same on any scale, and thus; For a uniaxial deformation λ:

$$S(q) = S_{iso}(\sqrt{\tilde{q}\tilde{\tilde{E}}\tilde{q}}) = S_{iso}(\lambda_q q) = S_{iso}[\sqrt{(\lambda^2\cos^2\varphi + 1/\lambda\sin^2\varphi)\,q^2}]$$

$$\langle\cos^2\theta\rangle = 2/(1 - 1/\lambda^3)\,(1 - (\mathrm{Arctg}\sqrt{(1-\lambda^3)})/\sqrt{(1-\lambda^3)})\,.$$

There exists a relation between the two quantities, though not simple, because $\langle\cos^2\theta\rangle$ is a complicated function of λ.

The second example is the junction affine network model [43] for a chain fixed only by its two ends to the network. In Sect. 7 it was pointed out that the whole form factor can be calculated [44]. In particular, the radius of gyration is [32], in a direction $\alpha = x, y, z$,

$$R^2_{g\alpha} = 1/(2N^2)\sum_i\sum_j\langle(\underline{R}_i - \underline{R}_j)^2\rangle = 1/2(N^2/N^2)\sum_n(1 - n/N)\,r_n^2$$

$$= R^2_{g\,iso}(1 + \lambda_\alpha^2)/2\,,$$

where $n = |i - j|$.

Ullmann [57] has also given the orientation function of the vector $\underline{r}_{ij}$ joining two monomers, which is for $i - j = 1$:

$$\langle\cos^2\theta\rangle = 1/(\sin^2\psi)\,(1 - \psi/\mathrm{tg}\,\psi)\,,$$

with $\sin\psi = (\lambda^2 - 1/\lambda)/(N - (\lambda^2 - 1))$.

It appears clearly that $\langle\cos^2\theta\rangle$ is a very slow function of λ if N is large (note the presence of N in the denominator of $\sin\psi$) while R_g is still a fast one. This reflects the well-known fact that the orientation of a monomer is much smaller than the orientation obtained for a totally affine deformation. Thus, $\langle\cos^2\theta\rangle$ is much less anisotropic than R_g in this example.

The third example is a case where the monomers are highly oriented on the small scale, but give on the large scale a correlation function which is oriented in the perpendicular direction. Finally, all models are *a priori* possible and no general phenomenological relation can be written without strong model statements.

However, it remains possible to compare qualitatively $S(q)$ and $\langle\cos^2\theta\rangle$ on the same scale, i.e. for the unit for length b, i.e. $q \sim 1/b$. For the junction affine model (example 2) for instance, the order of magnitude of $S(\tilde{q}_{per})/S_{iso}(\tilde{q})$ at $q \sim (1/10\ \text{Å})$ and of $P_2(\theta) = (3\langle\cos^2\theta\rangle - 1)/2$ is comparable. However, we here enter the region where the orientation effect is weaker than the usual accuracy of the SANS experiment. We will now report a recent experiment which compares the two quantities and is related to these problems.

15.2 Experimental Comparison of a Free Chain in a Strained Rubber

Two experiments have been performed which allow a comparison between $S(q)$ and $\langle\cos^2\theta\rangle$ for same conditions and the same sample. The form factor is given by SANS [58] and the orientation $P_2(\theta)$ by deuterium magnetic resonance [59]. Both are sensitive to deuterated species and can be used in melts for large deuterated fractions. A small chain of deuterated PDMS ($M_{nD} \sim 10000$, $M_{wD} \sim 20000$) is dissolved in a matrix of a non-deuterated PDMS endlinked network (mesh size identical to the labeled chain, 10000), simply by spreading and waiting a convenient time. The network is then uniaxially stretched and one observes the form factor of the labeled chain in all directions between q and the stretching axis on the two-dimensional detector. The result is that the form factor does not change for $1 < \lambda < 1.45$ and $3 \cdot 10^{-2}\ \text{Å}^{-1} < q < 4 \cdot 10^{-1}\ \text{Å}^{-1}$. It remains isotropic within an uncertainty of 3% and equal to the one of the isotropic sample within 10%. It has the classical features of the form factor of the Gaussian chain. On the other hand, the DMR result is that the frequency peak splits into two peaks separated by $\Delta\nu = 80$ Hz, which is the signature of an orientation effect. The splitting value is within 10% equal to the one observed, at same λ, for a deuterated PDMS chain of same molecular weight *endlinked* inside the network. SANS and DMR results could appear contradictory, but may be explained following several remarks:

— the orientation given by DMR is weak ($\Delta\nu = 80$ Hz $\rightarrow P_2(\theta) \sim 1.5 \cdot 10^{-3}$), i.e. under the precision of the SANS experiment. If the anisotropy is the same at any scale, as in an affine deformation and as would give a nematic field, this will not be detectable by SANS.

— a local anisotropy effect may even give less orientation on the large scale than on the small scale [58].

— these two cases are opposite cases to the rubbery deformation for which the orientation is larger when the length scale is larger. This latter is very neatly observable by SANS, meanwhile $P_2(\theta)$ is of the same order of magnitude in the NMR results.

This explanation also implies, besides a comparison of techniques, that the local anisotropy effect in rubbers on the scale of the monomer is more than not negligible compared to the orientation by end-to-end pulling of the endlinked chains, as already suggested [17].

16 Conclusion

It is shown that it is possible to obtain reproducible data for the single chain form factor during the relaxation from a stepstrain, and that current models allow the calculation of this form factor. A comparison experiment-theory is then possible. The conclusion of this comparison is still incomplete: the models, though simple, involve numerous processes requiring a large amount of data, of which only a part is available. Also it appears that the real situation is even more complex, as several simple predictions are not fitted, or at least that a large crossover regime is involved, increasing again the research field. More precisely, the strong results are that:

— there is agreement with the Rouse model at short times and disagreement at long times.
— there is no really strong evidence for reptation. For example:
  1) the retraction predicted by Doi and Edwards is not observed.
  2) the disengagement, which would lead to a characteristic behaviour of the form factor, could explain the data but is not fully determined because this requires a very long duration of relaxation for rather long chains.
  3) a matrix effect seems to appear in the range of 100000–1000000 more strongly than expected.
  4) additional relaxation is observed, in particular for large masses.

Point 1 appears to be elucidated and confirmed by long chains and shear data. For point 4, the degradation of the long chains must be reduced even further, although this would not suffice to cancel the effect. The same long *nondegradated* chains must be used at long times for point 2. For point 3, the essential need is for more data.

The most important experiments seem to be those using very long chains $> 2.5 \cdot 10^6$; such measurements are very rare even in classical rheology. It is to be emphasized that experiments on crosslinked melts are of great interest: first, to compare with melts; and second, intrinsically, as rubbers are a particular state of matter, the dynamics of which are still widely unknown, and for which theory is still approximate.

Other extensions need to be purposed: it is easy to improve the calculation of the form factor, e.g. by combining the now-available correct calculation for rubber classical theories with the one for reptation, and this for any direction with respect to the deformation axes (aspect of isointensity curves). On the level of scattering techniques, further stimulations will result from the exploration at smaller q, in particular owing to the availability of "ultracold neutrons" (i.e. a wavelength of up to 40 Å, achievable at ILL, Grenoble) for SANS and Spin Echo Inelastic Scattering. A coupling with other techniques is certainly useful (fluorescence polarisation, DMR, diffusion coefficient), as well as systematic and precise measurements of the stress coupled to any experiment.

Finally, extensions of the techniques to other materials are obvious. Some are straightforward if they involve a melt close to a glass transition or if they are very viscous; this depends only on the possibilities of the chemistry of deuteration: star and ring polystyrene, blends, ionomers, and possibly semirigid polymers and compatible copolymers. The use of other techniques (Sect. 2) would be required for more liquid materials, as multicomponent solutions, where again neutron scattering has no equivalent.

17 References

1. Boué, F., Nierlich, M., Leibler, L.: Polymer *23*, 9 (1982)
2. Edwards, S. F.: Proc. Roy. Soc. *9*, 92 (1967)
3. de Gennes, P. G.: J. Chem. Phys. *55*, 572 (1971)
4. Doi, M., Edwards, S. F.: J. Chem. Soc. Far. Trans. 2, *74*, 1802 (1978)
5. Doi, M.: J. Pol. Sci. Letters *18*, 775 (1980)
6. Oberthur, R. C.: Revue Phys. Appl. *19*, 663 (1984)
7. de Gennes, P. G.: J. Chem. Phys. *72*, 4756 (1980)
8. Hashimoto: IUPAC Proceedings, Washington, 1983
9. Boué, F.: These d'etat, Université Orsay Paris Sud, #2662 (1982)
10. Boué, F., Nierlich, M., Osaki, K.: J. Chem. Soc. Far. Symp. *18* (1983)
11. Boué, F., Cressely, R.: Lab. Leon Brillouin Report 1983
12. Ferry, J. D.: Viscoelastic Properties of Polymers, 3rd ed., Wiley, New York 1982
13. Daoud, M., de Gennes, P. G.: J. Pol. Sci., Pol. Phys. Ed. *17*, 1971, 1979; Klein, J.: Macromolecules *11*, 852 (1978)
14. Viovy, J. L.: J. Physique, *46*, 847 (1985)
15. de Gennes, P. G.: J. Phys. *36*, 1191 (1975); Klein, J.: J. Chem. Soc. Far. Symp. *18*, (1983); Helfand, E., Pearson, D. S.: Macromolecules, *17*, 888 (1984)
16. Tassin, M., Monnerie, L.: J. Pol. Sci., Pol. Phys. Ed. 1983 or 1984
17. Monnerie, L.: J. Chem. Soc. Far. Trans. *18*, (1983)

17bis. Montfort, J. P.: These d'Etat Université de Pau et Pays de l'Adour 1984 (to be published)

18. Graessley, W. W.: Adv. Pol. Sci. *47*, 68–117 (1982)
19. Marucci: Macromolecules *14*, 434 (1981) (and paper submitted)
20. Boué, F., Nierlich, M., Jannink, G., Ball, R. C.: J. Physique *43*, 137–148 (1982)
21. Allen, G., Higgins, J. S., Macconachie, A.: Far. Trans. 2, *72*, 2117–2130 (1982)
22. Marin, G.: Thèse d'État, Université de Pau et Pays de l'Adour, 1978 and papers by Marin, G., Graessley, W. W., 1978–1979
23. Picot, C., Duplessix, R., Decker, D., Benoit, H., Boué, F., Cotton, J. P., Daoud, M., Farnoux, B., Jannink, G., Nierlich, M., de Vries, A. J., Pincus, P.: Macromolecules *10*, 436 (1977)
24. Boué, F.: 3rd cycle Thesis, Université Louis Pasteur, 1977, and Boué, F., Jannink, G.: Physique, Colloques C2 (supplem. to #6) *39*, C2–183 (1978)
25. Macconachie, A., Allen, G., Richards, R. W.: Polymer *22*, 1157 (1981)
26. Boué, F., Nierlich, M., Jannink, G., Ball, R. C.: J. Physique Lettres L582–L589 and L590–L593 (1982)
27. Hadzioannou, G., Hui Wang, Li, Stein, R. S., Porter, R. S.: Macromolecules *15*, 880–882 (1982)
28. Boué, F., Osaki, K.: (to be published)
29. Bastide, J., Boué, F., Herz, J.: J. Phys. *46*, 1967–1979 (1985). More data on deswollen rubbers are in Ref. 29bis.

29bis. Bastide, J.: in Physics of Finely Divided Matter, Springer Proc. in Phys. *5*, Daoud, M., Boccava, N., Eds., Springer (1985)

30. Boué, F., Nierlich, M., Jannink, G.: ILL Report 1978
31. Boué, F.: ILL report 1984 (and to be published)
32. Muller, Froehlich: (private communication)
33. Kirste, R. C., Oberthur, R. C.: "Small Angle X-ray Scattering", Chapt. 12, Glatter, O., Kratky, O. (Eds.), Academic Press, London 1982
34. Tobolsky, A. V.: J. Appl. Phys. *27*, 673 (1956)
35. Wignall, G. D., Ballard, D. H., Schelten, G.: Eur. Pol. J. *10*, 861 (1974); Cotton, J. P., Decker, D., Benoit, H., Farnoux, B., Higgins, J. S., Jannink, G., Ober, R., Picot, C.: J. des Cloizeaux, Macromolecules *7*, 863 (1974)
36. Daoudi, S.: J. Physique *38*, 731 (1977)
37. Hong, Noolandi, I.: J. Physique *45*, L149–L157 (1984)
38. de Gennes, P. G.: J. Physique *41*, 735–740 (1981)
39. Boué, F., Osaki, K., Ball, R. C.: J. Pol. Sci., Polym. Phys. Ed., *23*, 833–844 (1985)
40. de Gennes, P. G., Leger, L.: Rev. Ann. Phys. Chem., 1982
41. Benoit, H., Duplessix, R., Ober, R., Daoud, M., Cotton, J. P., Farnoux, B., Jannink, G.: Macromolecules *8*, 451 (1975)

42. Kuhn, W., Kunzle, O., Katchalsky, A.: Helv. Chim. Acta *31*, 1994 (1948)
43. Kuhn, V. W., Grunn, F.: Kolloid Zeitschrift, p. 248, 1942; Wall, F. T., Flory, P. J.: J. Chem. Phys. *19*, 1435 (1951)
44. Ullmann, R.: Macromolecules *15*, 1395 (1982)
45. Pearson, D. S.: Macromolecules *10*, 698 (1977)
46. James, H., Guth, E.: J. Chem. Phys. *19*, 1435 (1951); Deam, R. T., Edwards, S. F.: Phil. Trans. Roy. Soc., Ser. A *280*, 317 (1976)
47. Warner, M., Edwards, S. F.: J. Phys. A *11*, 1649 (1978)
48. Flory, P. J., Erman, B.: Macromolecules *15*, 800–806 (1982)
49. Boué, F., Bastide, J.: ILL report 1984 (and to be published). See also Reference 49bis.
49bis. Boué, F., Bastide, J.: Gomadingen meeting on Polymer Network, J. Coll. & Pol. Sci. (1987)
50. Marucci remarked that the application of the Doi-Edwards model for the relation between stress and deformation leads to an unstable situation and therefore inhomogeneities.
51. Osaki, K., Kurata, M.: Macromolecules *13*, 671 (1980)
52. Osaki, K., Doi, M.: Pol. Eng. Reviews *4*, 35–71 (1984)
53. de Gennes, P. G.: Scaling Concepts in Polymer Physics, Cornell University Press, Ithaca 1978
54. Farnoux, B.: Annales de Physique *1*, 73 (1976); Cotton, J. P., Decker, D., Farnoux, B., Jannink, G., Ober, R., Picot, C.: Phys. Rev. Lett. U32J, 1170 (1976)
55. Rawiso, M., Duplessix, R., Picot, C.: Macromolecules *20*, 630 (1987)
56. Dubault, A., Deloche, B.: (submitted to Polymer); Deloche, B., Lapp, A., Herz, J.: J. Physique Lettres *43*, L-763 (1982)
57. Ullman, R.: Macromolecules *11*, 987–989 (1987)
58. Boué, F., Bastide, J., Lapp, A., Picot, C., Farnoux, B.: Europhys. Lett. *1* (12), 637–645 (1986)
59. Dubault, A., Deloche, B.: (published in same issue as (58))
60. Bastide, J., Boué, F.: Physica *140A*, 251–260 (1986)
61. Rawiso, M., Boué, F.: to be published.
62. More precisely, χ is $2 \cdot 10^{-4}$ for the couple polystyrene monomer-deuterated polystyrene monomer. The upper limit for a stable one phase mixture (value at the spinodal) is

$$\chi_s = \frac{1}{2}\left[\frac{1}{N_H\phi_H} + \frac{1}{N_D\phi_D}\right],$$

where $N_H(N_D)$ is the number of monomers and $\varphi_H(\varphi_D = 1 - \varphi_H)$ the volume fraction of the H(D) species. In the case $\varphi_H = \varphi_D = 50\%$, $N_H = N_D$, $\chi < \chi_s$ when $N_H < 10^4$, i.e. $M < 10^6$; but if $\varphi_D = 10\%$, the stability condition for $N_H = N_D$ becomes $M \lesssim 2.5 \cdot 10^6$. The formula for the scattering is [1)]

$$\frac{1}{S(q)} = \frac{1}{\varphi_H S_H(q)} + \frac{1}{\varphi_D S_D(q)} - {}^2\chi$$

so that χ can be neglected except for large mastes at $qR_g < 1$ ($S_H(q) \to N_H(1 - q^2R_g^2/3)$). Limit cases are currently under study. Values for χ are given by: C. Strazielle, H. Benoit; A. Lapp, from data of Ref. 1 for PS); Bates and Wignall, Macromolecules, 1986.